

Detecting Concussion History in Athletes Using Pose Estimation and Machine Learning

William James Robert Alves

A Thesis

In The Department of

Computer Science & Software Engineering

Presented in Partial Fulfillment of the Requirements
for the Degree of Master of Applied Science (Software Engineering)

at Concordia University
Montreal, Quebec, Canada

June 2024

© William James Robert Alves, 2024

CONCORDIA UNIVERSITY
School of Graduate Studies

This is to certify that the thesis prepared

By: William James Robert Alves

Entitled: Detecting Concussion History in Athletes using Pose Estimation and Machine Learning

and submitted in partial fulfillment of the requirements for the degree of

Master of Applied Science (Software Engineering)

complies with the regulations of the University and meets the accepted standards with respect to originality and quality.

Signed by the final Examining Committee:

_____ Chair and Examiner

Dr. Sudhir Mudur

_____ Examiner

Dr. Yiming Xiao

_____ Supervisor

Dr. Thomas Fevens

Approved by _____

Leila Kosseim, Graduate Program Director

Department of Computer Science and Software Engineering

June 21, 2024 _____

Dr. Mourad Debbabi, Dean

Faculty of Engineering and Computer Science

Abstract

Detecting Concussion History in Athletes using Pose Estimation and Machine Learning

William James Robert Alves

Concussions present a significant risk to athletes, with females exhibiting higher rates and prolonged recovery times than males. Current sideline concussion detection methods, such as the King-Devick test, suffer from validity issues, especially among young athletes, highlighting the need for more accurate and objective assessment tools. This study investigates the feasibility of using pose estimation technology, specifically Microsoft Kinect V2, to assess postural stability in varsity athletes with a concussion history. Inspired by previous research utilizing force plates, our study analyzes video recordings of athletes performing specific exercises to detect dynamic balance deficits. In a cross-sectional study of 444 varsity athletes in 2022 and 464 varsity athletes in 2023, results reveal significant differences in movement mechanics between concussed and control groups, with the Drop Vertical Jump (DVJ) exercise demonstrating the highest discriminatory power. Notably, concussed individuals exhibit longer time to stabilization (mean difference = 0.089 seconds, $p = 0.046$) during DVJ, indicating potential lingering balance impairments. While single leg squat and single leg hop exercises showed fewer discriminatory metrics than DVJ, they still provide valuable insights into balance capabilities. The DVJ was the most effective at distinguishing between injured and healthy male athletes, while the SLH was more effective for females and the SLS was equally ineffective for both males and females. Our research also studied 20 varsity athletes who sustained one or many concussions from 2022 to 2023 and compared their DVJ exercise metrics before and after injury. The results of this prospective study demonstrated few statistically significant differences between their 2022 and 2023 jumps for all computed metrics, suggesting that the occurrence of concussion(s) did not have a significant measurable impact on the athletes' jumping mechanics or dynamic balance for the DVJ over this period.

Acknowledgments

I thank Dr. Thomas Fevens for his tremendous guidance throughout my research. From the beginning, Dr. Fevens established a relaxed culture where I felt comfortable sharing ambitious ideas, which allowed for a productive working relationship. It was truly a joy to have him as my supervisor. I would also like to extend my thanks to Dr. Paul Martineau and his research team for providing me with such a comprehensive dataset to work with from day one. Without Dr. Martineau and the rest of the research team it would have taken me much longer to accomplish my research goals. Of particular importance to my success was Athanasios Barbouras who has worked on the KITS project for six years and counting. Athanasios introduced me to the KITS architecture and guided me through the process. He provided assistance whenever I was confused, and I am deeply grateful for his tremendous efforts.

Finally, I would like to thank my parents and girlfriend, Danielle, for providing me with tremendous support, especially early on when there was so much doubt. Embarking on a software engineering research project was daunting coming from a background in mechanical engineering and I would not have the confidence I have today without the help of my loved ones.

Table of Contents

List of Figures	vii
List of Tables	ix
Chapter 1 Introduction	1
1.1 Motivation.....	1
1.2 Problem Statement	2
1.3 Important Contributions and Challenges	3
1.4 Organization.....	4
Chapter 2 Background	5
2.1 Human Pose Estimation.....	5
2.2 Mild Traumatic Brain Injury and Persistent Long-Term Concussion Symptoms	9
2.3 Detecting Concussions and Balance with Pose Estimation Cameras & Force Plates ..	12
2.4 Classical Machine Learning Techniques	18
Chapter 3 Data Description & Methodology	22
3.1 Description of Performed Exercises	23
3.2 Comparing 2022 and 2023 Datasets	25
3.3 Data Capture and Processing Methodology.....	26
3.3.1 Time-Series Joint Information	26
3.3.2 Time-Series Ground Reaction Forces	29
3.3.3 Exercise Metrics.....	31
3.3.4 TBCM Sway Implementation	33
3.3.5 Time to Stabilization.....	34
Chapter 4 Results & Discussion	37
4.1 Leg Dominance Outcomes.....	37
4.2 DVJ, SLS, SLH Cross-Sectional Study Overall Outcomes	37
4.3 DVJ, SLS and SLH Cross-Sectional Gender-Based Outcomes.....	42
4.4 DVJ Prospective Analysis Outcomes	45
4.5 Feature Selection by Machine Learning Classifiers	53
Chapter 5 Conclusions and Future Work.....	60

Bibliography 62

List of Figures

Figure 1 BESS Test Different Stances [8]	2
Figure 2 Representation of Coronal and Sagittal Planes	5
Figure 3 Examples of Human Pose Estimation [10].....	6
Figure 4 Kinect V2 Sensor Diagram.....	6
Figure 5 Kinect V2 Depth Image Capture	7
Figure 6 Depth Accuracy Error Distribution of Kinect V2 [16].....	9
Figure 7 Double-Limb Jump Landing Sequential Motion [32].....	11
Figure 8 Time to stabilization during the single leg hop for both groups: A, on the dominant leg, and B, on the nondominant leg. a Indicates a between-groups difference ($F_{2,27} = 5.69$, $P = .02$) [37]......	14
Figure 9 (A) The Kinect-Driven musculoskeletal model, (B) 25 contact points under the foot, (C) musculoskeletal model working during one gait trial with calculated GRF [39]......	15
Figure 10 Ensemble curves (mean and 90% confidence intervals) of the measured vs calculated GRF in all directions [39].	16
Figure 11 Typical Architecture of an MLP [49].....	18
Figure 12 Two-Dimensional Example of SVM Maximum Margin Classifier (boundary = green line) [50]......	19
Figure 13 Simple Example of Decision Tree used for Deciding whether to play Golf [53]	20
Figure 14 % Split of Varsity Sport for All Athletes - 2022 Data (N = 444).....	22
Figure 15 % Split of Varsity Sport of All Athletes - 2023 Data (N = 464).....	23
Figure 16 Sequence of motion of DVJ. (A) Initial Resting Position, (B) First Landing, (C) Maximal Vertical Jump, (D) Second Landing.....	23
Figure 17 Sequence of Motion of SLS: (A) First One Leg Standing Position, (B) First Squat Full Flexion, (C) Second One Leg Standing Position, (D) Second Squat Full Flexion.....	24
Figure 18 Sequence of Motion for a SLH. (A) Initial Single Leg Balancing Position, (B) Forward Jump Phase, (C) Landing Phase.....	24
Figure 19 (A) Coronal Knee Angle and (B) Sagittal Knee Angle	27
Figure 20 (A) Spine Sway X shown by angle between vertical line and spine, Pelvis Tilt Y shown by large sweeping arrow, (B) Spine Sway Z shown by angle between vertical line and spine, Pelvis Tilt Z shown by large sweeping arrow.	28
Figure 21 (A.1) Neck Sway X, (A.2) Wrist Distance, (A.3) Ankle Distance and (B) Neck Sway Z	29
Figure 22 Actual vs Predicted Ground Reaction Forces using six different regression models for the second landing of the DVJ.	30
Figure 23 Actual vs Predicted Ground Reaction Forces using six different regression models for the first squat of the SLS.....	30
Figure 24 TBCM point (red) implementation in KITS software.....	34
Figure 25 Example of Computation of Actual vs Predicted TTS for a DVJ	36
Figure 26 Prospective Study Data Flow Chart Breakdown	46

Figure 27 Mean Max Spine Sway Landing Ratio X compared across years (2022 and 2023) for those who did not sustain a concussion from year to year and those who did (-0, -1) and those who had no previous concussion history and those who did (-NC, -C). 48

Figure 28 Mean Maximum Neck Sway X compared across years (2022 and 2023) for those who did not sustain a concussion from year to year and those who did (-0, -1) and those who had no previous concussion history and those who did (-NC, -C). 49

Figure 29 IJV Spine Sway X Variability compared across years (2022 and 2023) for those who did not sustain a concussion from year to year and those who did (-0, -1) and those who had no previous concussion history and those who did (-NC, -C). 51

Figure 30 IJV Maximum spine sway landing ratio X compared across years (2022 and 2023) for those who did not sustain a concussion from year to year and those who did (-0, -1) and those who had no previous concussion history and those who did (-NC, -C). 52

Figure 31 IJV Maximum ankle distance compared across years (2022 and 2023) for those who did not sustain a concussion from year to year and those who did (-0, -1) and those who had no previous concussion history and those who did (-NC, -C). 53

Figure 32 Balanced Accuracy (%) for each classifier for feature selection process (DVJ) 55

Figure 33 Balanced Accuracy (%) for each classifier for feature selection process (SLS) 56

Figure 34 Balanced Accuracy (%) for each classifier for feature selection process (SLH) 58

List of Tables

Table 1 2022 Varsity Sport % Split and per-sport Average Weight (kg), Average Height (m) and Average Age	25
Table 2 2023 Varsity Sport % Split and per-sport Average Weight (kg), Average Height (m) and Average Age	26
Table 3 Mean MSE (N) between actual GRF and predicted GRF for all test examples in all three force directions for DVJ, (Second Landing) SLS and SLH (start to toe-off phase).....	31
Table 4 Common Exercise Description	32
Table 5 Exercise-Specific Metrics Description	33
Table 6 TTS P-Value for different K values for all exercises	35
Table 7 Average and Median Percentage Change between Actual TTS (s) and Predicted TTS (s) for each model.....	36
Table 8 Leg Dominance Statistics for 2022 and 2023 athletic cohorts	37
Table 9 Drop Vertical Jump Outcomes (statistically significant metrics shown by bolded rows)	37
Table 10 Single Leg Squat Outcomes (statistically significant metrics shown by bolded rows) .	39
Table 11 Single Leg Hop Outcomes (statistically significant metrics shown by bolded rows) ...	40
Table 12 Comparison of Metrics Between Control and Concussion Groups by Gender for DVJ (Statistically Significant Metrics shown by Bolded Rows)	42
Table 13 Comparison of Metrics Between Control and Concussion Groups by Gender for SLS (Statistically Significant Metrics shown by Bolded Rows)	42
Table 14 Comparison of Metrics Between Control and Concussion Groups by Gender for SLH (Statistically Significant Metrics shown by Bolded Rows)	44
Table 15 Prospective Study Mean Outcomes (DVJ), all metrics computed in degrees except for ratios which are unitless and time to stabilization which is in seconds.	47
Table 16 Prospective Study IJV Outcomes (DVJ), all metrics computed in degrees except for ratios which are unitless and time to stabilization which is in seconds.	50
Table 17 Machine Learning Classifier Results for DVJ (binary classification task)	54
Table 18 Best Features for MLP Classifier (DVJ).....	55
Table 19 Machine Learning Classifier Results for SLS Dominant Leg (binary classification task)	56
Table 20 Best Features for RF Decision Tree Classifier (SLS).....	57
Table 21 Machine Learning Classifier Results for SLH Dominant Leg (binary classification task)	58
Table 22 Best Features for RF Decision Tree Classifier (SLS).....	59
Table 23 Classification Report for KNN using top three features (SLH).....	59

Chapter 1 Introduction

1.1 Motivation

Concussions are a major form of injury for athletes of all ages and sex. In fact, concussions greatly affect the vulnerable female population, with females having 1.4 times higher overall concussion injury rates than males. Furthermore, female athletes also display more time loss after concussion than men [1]. The current solutions to detect concussions in athletes during game time are inaccurate. The King-Devick (K-D) test for concussion detection is a popular method for detecting concussions on the sideline. The K-D test is a visual performance test that can be easily administered on the sidelines. The flaw in this test comes from athletes purposely botching their baseline tests so that they can later pass their K-D assessment in the event they have a concussion, this is widely referred to as “sandbagging” [2]. “In a cross-sectional study of 7897 participants who completed baseline neurocognitive testing for the management of sport-related concussion, 56% failed at least 1 of 4 published validity indicators” [1]. The study also highlights that 3 of 4 young athletes ages 10-12 failed validity indicators, suggesting that the current methods for baseline concussion testing are invalid for young vulnerable athletes [1]. The inaccuracy of the current methods of baseline concussion testing demonstrates the need for an affordable, non-invasive, efficient, and more accurate solution for concussion testing.

The prevalence of athletes who exhibit long term post-concussion symptoms (PCS) is not insignificant. In fact, a prospective analysis of 110 injured patients and 32 healthy participants showed that injured patients demonstrated a higher cumulative post-concussion symptom score than the healthy controls even after a mean time of 2.9 years after being diagnosed with their mild traumatic brain injury (mTBI) [3]. Furthermore, studies have shown that neck pain and neck stiffness are common long-term symptoms of concussion along with changes in balance measures in the acute and chronic phases of concussion [4], [5]. The Balance Error Scoring System (BESS) is a widely accepted test for scoring postural stability, often used in the athletic population with concussion or mTBI. The test consists of three positions, a double-leg stance with hands on hips and feet, a single leg stance standing on nondominant leg with hands on hips and a tandem stance with the nondominant foot behind dominant foot. The illustration of the aforementioned standard BESS positions can be found in Figure 1. A trained evaluator scores the test by counting the number of errors observed using an objective list of errors [6]. Studies have shown that balance difficulties were present in 80% of children with concussions using the BESS test along with physical examination measures [7].

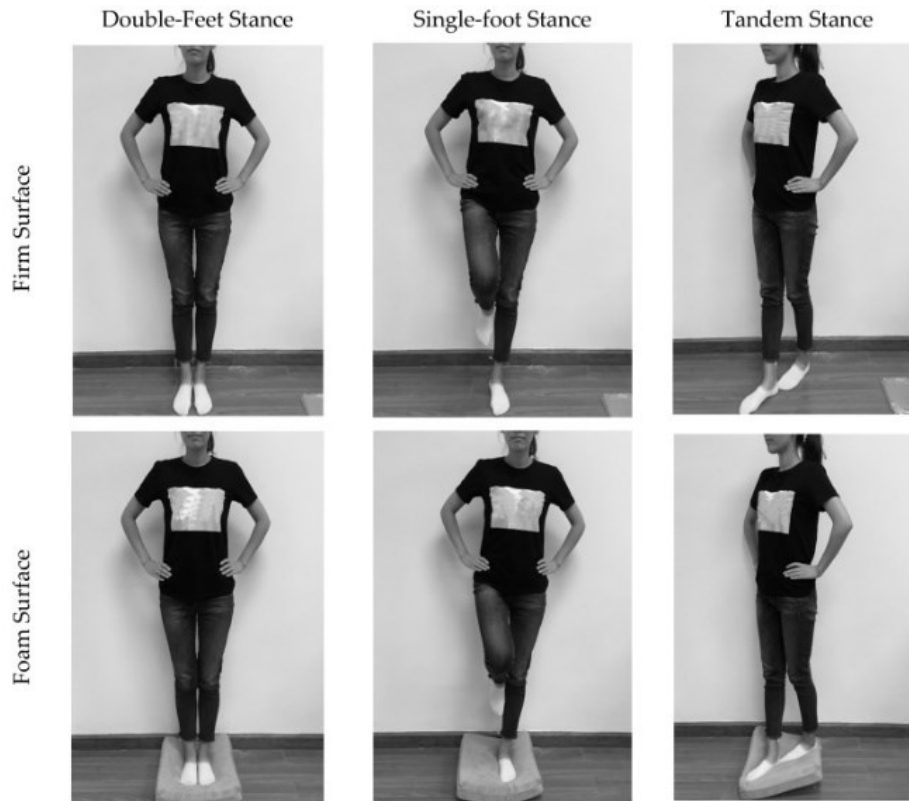


Figure 1 BESS Test Different Stances [8]

Relying on a human interpreter to assess balance using the BESS test presents some subjective limitations due to the inherent nature of the BESS test. The subjective nature of the BESS test motivates an objective alternative in assessing postural stability. Assessing postural stability and balance using pose estimation sensors has been made possible thanks to the Microsoft Kinect camera and other pose estimation hardware. In fact, measuring postural stability using Microsoft's Kinect V2 camera has shown to have excellent correlation coefficients to the human rater's BESS scores ($r = 0.93$, $p < 0.05$) and test-retest reliability ($ICC = 0.81$, $p > 0.05$) [8]. The Kinect camera's excellent potential for objectively assessing postural stability in athletes makes it a strong candidate in creating an affordable, non-invasive, efficient, and more accurate solution for concussion symptom testing.

1.2 Problem Statement

The purpose of the research is to investigate whether it is possible to detect a history of concussion in varsity athletes using simple pose estimation video recordings of athletes performing specific plyometric exercises. Classical machine learning methods (supervised and unsupervised) such as regression and logistic regression classifiers such as Support Vector Machines (SVMs), K -Nearest Neighbors (KNN), Multi-layer Perceptron (MLP) and Decision Trees to group and classify the members of the examined cohort of athletes on concussion history will also be explored.

This research is powered by a comprehensive dataset provided by the Research Institute of the McGill University Health Centre (RI-MUHC) containing a homogeneous group of over 900 highly skilled varsity athletes who play a wide variety of sports from McGill and Concordia University in Montreal, QC. All these athletes have performed specific plyometric exercises including the drop vertical jump (DVJ), single leg squat (SLS) and single leg hop (SLH) in front of a Kinect pose-estimation camera for the 2022 and 2023 preseasons. Throughout the two years, each athlete has performed roughly 7-12 total plyometric exercises each in front of the camera resulting in a total number of recordings of over 10,000 from the past two years. The data processing software is an internally developed software by the name of Kinect Intelligent Tracking System (KITS). For each exercise, KITS provides over twenty metrics tailored to the specific exercise the athlete is performing. The data also contains in-depth information about the athlete's concussion history. This study draws inspiration from research conducted by Lynall et al., who investigated the presence of dynamic balance deficits in individuals with a history of concussion sustained within the past two years. They compared these individuals with control participants regarding their performance in the single leg hop and single leg squat exercises. The study employed time to stabilization (TTS) and other metrics, computed using force plates, as the primary measures. The results of their experiment demonstrated that the concussed group had a longer TTS than the control group during the single leg hop on the nondominant leg (mean difference = 0.35 seconds [95% confidence interval = 0.04, 0.64], $p = 0.02$). No TTS differences were observed for the dominant leg ($p = 0.43$), and no group differences were observed for the single leg squat on either leg ($p = 0.11$) [37]. The methods in the paper by Lynall et al. require an advanced and expensive kinesiology laboratory to determine if a patient exhibits balance impairments due to the use of force plates. Our research aims to analyze the statistics of recently concussed varsity athletes and a control group derived from our pose estimation software to ascertain any notable distinctions in their movement mechanics and balance capabilities and assess which exercise most exemplifies these distinctions.

1.3 Important Contributions and Challenges

The biggest challenge throughout the course of my research was deciphering how to chart the correct path to producing meaningful research results. This challenge was at the forefront during the first few months of my research. In the first months, I had no idea where to start. There were hundreds of avenues to explore and understanding which of them is the most optimal was an almost impossible and overwhelming task. After discussions with my supervisor, Dr. Fevens, he told me to just get started analyzing the data in any way I see fit. I started down this suggested path and began to get my feet dirty with the data and the data processing methodology. The next steps were to figure out a meaningful research path- a scientifically robust way of answering the question: "can we detect concussion symptoms in athletes using a pose estimation device?". This was the most difficult question to adequately answer and required extensive research to garner "light bulb" ideas which would help us to solve our ultimate problem. It was not until the month of March, around four months into my full-time research, where I charted a path to produce robust scientific results to satisfy a yes or no answer to our question. After discovering the time to stabilization results using force plates by Lynall et Al., our innovative idea was to produce the same experiment through estimating ground reaction forces using our pose estimation data and machine learning regression models. We knew that if the regression models proved accurate, we can conduct a

similar analysis between recently injured and healthy controls and see if the time to stabilization differences hold with our pose estimation and machine learning approach at computing balance metrics without force plates. Therefore, we believe that our most important contribution to our academic field is being the first to utilize specific joint pose estimation data to accurately estimate ground reaction forces using random forest decision tree regression modelling.

1.4 Organization

The remainder of this research is organized as follows:

In Chapter 2, we present a literature review including the science behind human pose estimation with particular emphasis on Microsoft's Kinect V2 pose estimation camera. Furthermore, chapter 2 will present pertinent literature on methods for detecting balance impairments using pose estimation cameras and other mediums. Finally, chapter 2 will provide a brief literature review on the many machine learning algorithms used throughout the research.

Chapter 3 explains the 2022 and 2023 varsity athlete datasets, the difference between them and the breadth of concussion information contained in them. The data capture methodology of the three plyometric exercises (drop vertical jump, single leg hop, single leg squat) will be explained along with an in-depth review of time-series data and exercise metrics outputted by KITS.

Chapter 4 goes through the many results and discussions including a prospective study of athletes from 2022 and 2023 who performed drop vertical jumps and a cross-sectional study comparing exercise metrics for the drop vertical jump, single leg squat and single leg hop exercises. A study exploring the performance of different machine learning classifiers will be explored.

Chapter 5 concludes the study by summarizing the experiment's results whilst also providing insights on future work.

Chapter 2 Background

Computer vision is a branch of artificial intelligence (AI) that utilizes machine learning and neural networks to extract significant information from digital images, videos, and other visual inputs. Essentially, computer vision allows computers to recognize objects, people, animals, and places, interpreting them in a meaningful way similar to human perception. [9]. The process of assigning labels to millions of images has allowed this field of machine learning and computer vision to flourish in the last decade. Computer scientists have been able to leverage the enormous dataset of labelled images to perform accurate human pose estimation (HPE).

2.1 Human Pose Estimation

HPE is an accurate and cost-effective way to capture movement of people in a scene (video imaging) and detect 3-Dimensional key point joint information in space (x, y and z coordinates) [10]. Examples of possible tracked key points include the ankle, hip, wrist, elbow, shoulder, head, neck and many others. The 3D key points can be used to identify motion patterns, specific joint position, knee angles including coronal and sagittal plane angles (as shown in Figure 2), neck sway, spine sway, hand velocity, ankle separation distance and a multitude of other metrics by use of simple vector mathematics [12]. Human pose estimation has been used in action recognition, animation, gaming, sports medicine, musculoskeletal injury prevention, autonomous navigation and many other applications [10], [11].

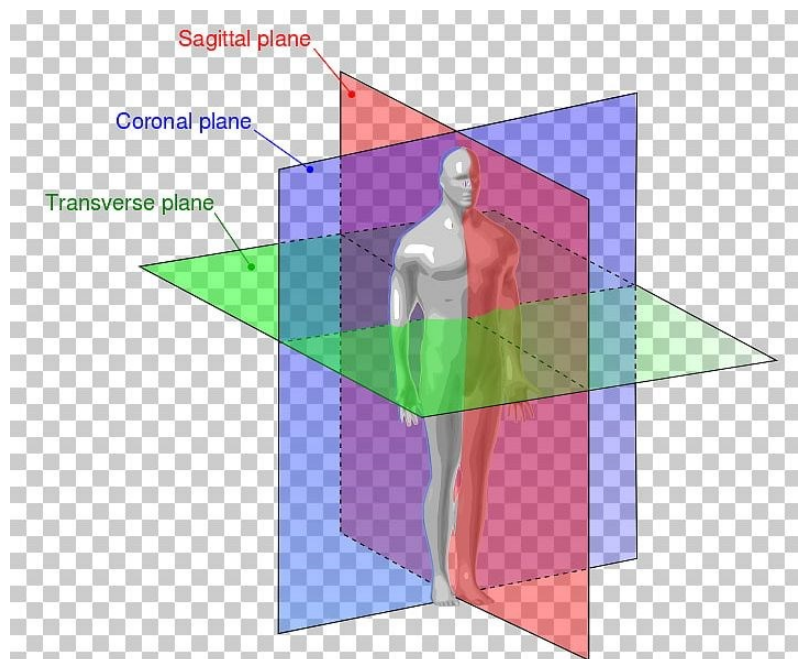


Figure 2 Representation of Coronal and Sagittal Planes

Current state-of-the-art human pose estimation algorithms have been trained using large datasets of digital images and videos of human movement which joint information/location has

been labelled manually [13]. This dataset contains a breadth of images of diverse human poses and clothing types in the effort of capturing both common and rare human poses. The trained algorithms can track new, unlabeled joints when capturing a human body. Figure 3 represents examples of active human pose estimation algorithms at work tracking multiple key points in space.

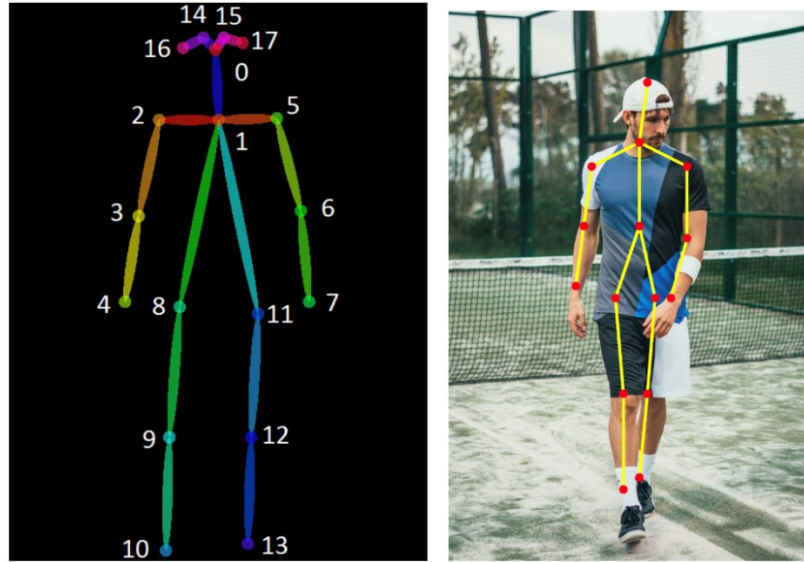


Figure 3 Examples of Human Pose Estimation [10]

The Microsoft Kinect Camera V2 is a state-of-the-art pose estimation camera developed in 2012. The Kinect V2 uses a 3-axis accelerometer as its motion sensor, a 1920 x 1080 RGB camera with a refresh rate of 30 frames per second. To get full pose estimation imaging, the Kinect camera is equipped with a Time-of-Flight depth camera with a resolution of 512 x 424 at a refresh rate of 30 frames per second [14]. Figure 4 shows a diagram of a Kinect V2 sensor.

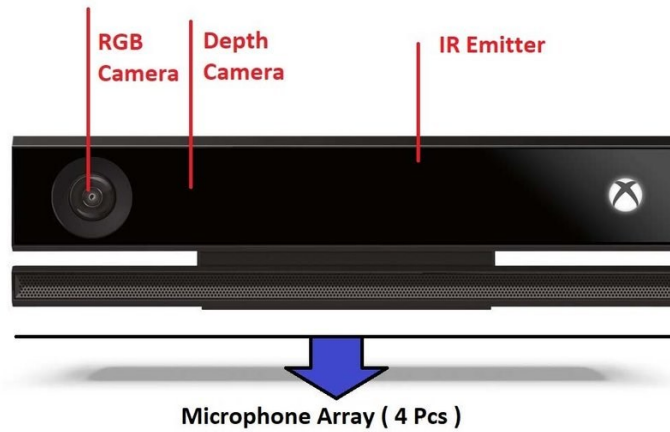


Figure 4 Kinect V2 Sensor Diagram

A 3D time of flight (TOF) camera works by illuminating the scene with a modulated light source, observing the reflected light and interpolating distance measures through the reflected light source [61]. TOF sensors measure distance at every pixel respective to the resolution of the depth

sensor and upscale to the resolution of the RGB camera, resulting in a depth map. Depth values are represented as 16-bit unsigned integer values where the larger the value, the further the object is from the Kinect camera. This output is represented as a black and white image where the brighter the color represents an object further away from the camera as shown in Figure 5.



Figure 5 Kinect V2 Depth Image Capture

Inferring body position is a two-stage process. Firstly, the Kinect V2 camera computes a depth map using structured light then infers body position using machine learning classification. The general principle of structured light is to project a known pattern onto the scene and infer depth from the deformation (or resolution differences) of that pattern. The pattern that the Kinect V2 projects onto the screen is a speckle pattern of infrared laser light. The Kinect V2 captures depth information through the basic principle that further away objects “seem blurrier” than closer objects. The Kinect V2 captures depth information based on the principle that distant objects appear "blurrier" than those closer. It uses a special astigmatic lens with different focal lengths along the x and y axes, causing a projected circle to become an ellipse. The orientation of this ellipse varies depending on the depth at which it is projected in space. The Kinect's backend software then translates the ellipse's orientation into a depth measurement [15].

The second phase of the Kinect's pose estimation capabilities is inferring body parts using a randomized decision forest learned from over one million training examples. Pose estimation research was often limited by the number of training examples available since creating realistic images through computer generated techniques is problematic due to the huge color and texture variability induced by clothing, hair and skin [17]. The key advancement in machine learning for the classification of body parts was made possible through the generation of synthetic data. Shotton et Al. were able to accomplish this ambitious feat by randomly sampling a pose from their in-house motion capture database, then using standard computer graphics techniques to render depth. The pose is then retargeted to a set of fifteen base meshes which have their own weight and height variability. Additional training examples are generated by rotating and translating the character in the scene, uniformly at random. On top of that, a multitude of mesh models of hair styles and items of clothing are chosen at random to finalize the generation of realistic synthetic images [17].

Microsoft utilized this synthetic image generation pipeline to obtain over a million training examples to power their random forest decision tree classifier used in the Kinect hardware [15]. The decision tree algorithm is a simple, yet efficient supervised machine learning technique used for both classification and regression. A decision tree algorithm works by continuously splitting the data points according to certain parameters specific to the problem that is being solved [18]. For example, in the problem of deciding whether or not to play golf that day, a decision tree could “ask” the data certain basic questions such as “already raining?”, “humid”, “cloudy?”, all of which have binary yes/no answers associated with them. Through the data’s response to these many questions, the algorithm will output a probabilistic or binary prediction on whether one is likely or unlikely to play golf based on copious amounts of training data the algorithm has previously been trained on [15]. An example of a decision tree question that Shotton et Al. would use for the classification of body parts in an image would be “how does the (normalized) depth at the pixel in image A compared to the pixel in image B” [17]. There are too many possible questions to ask, therefore, to increase algorithm efficiency, Kinect uses a random selection of 2000 questions each time it trains. Random forest decision trees may be tailored to output a binary classification. The Kinect was trained to output a probabilistic output when training [17]. For more information on the machine learning techniques used in this research please refer to section 2.4.

The accuracy of the depth imaging and pose estimation capabilities of the Kinect have been evaluated and assessed by many researchers. The Kinect is limited by problems of occlusion, where the view of body parts may be obstructed by objects or self-occlusion where certain body parts are hidden behind other parts of the tracked body [19]. Self-occlusion is especially a problem when a tracked subject is performing complicated plyometric exercises. In a study which pitted the Kinect against the Vicon motion capture system, they concluded that the Kinect V2 sensor is able to offer “state-of-the-art head pose estimation in real time without the need for calibration” [19]. Furthermore, a paper examining the accuracy of the Kinect’s depth sensor outlined several forms of noise such as edge noise and structural noise. Edge noise occurs along the edges of an object when it has a sharp contour, leading to depth measurement errors for sharp objects. Structural noise occurs when a planar surface is pointed perpendicular towards the depth camera, but the camera is unable to capture a perfectly flat surface. An additional limitation was found when a reflective object such as a mirror or a window was placed within the field of view of the Kinect since the IR emitter cannot be reflected back to the camera. This phenomenon is shown in Figure 5 where a window is in the background of the scene (furthest away) but is being displayed in black which translates to a close-up object. Despite these limitations, the Kinect proved to have excellent depth accuracy when the object or human was placed within the green region as defined in Figure 6 [16].

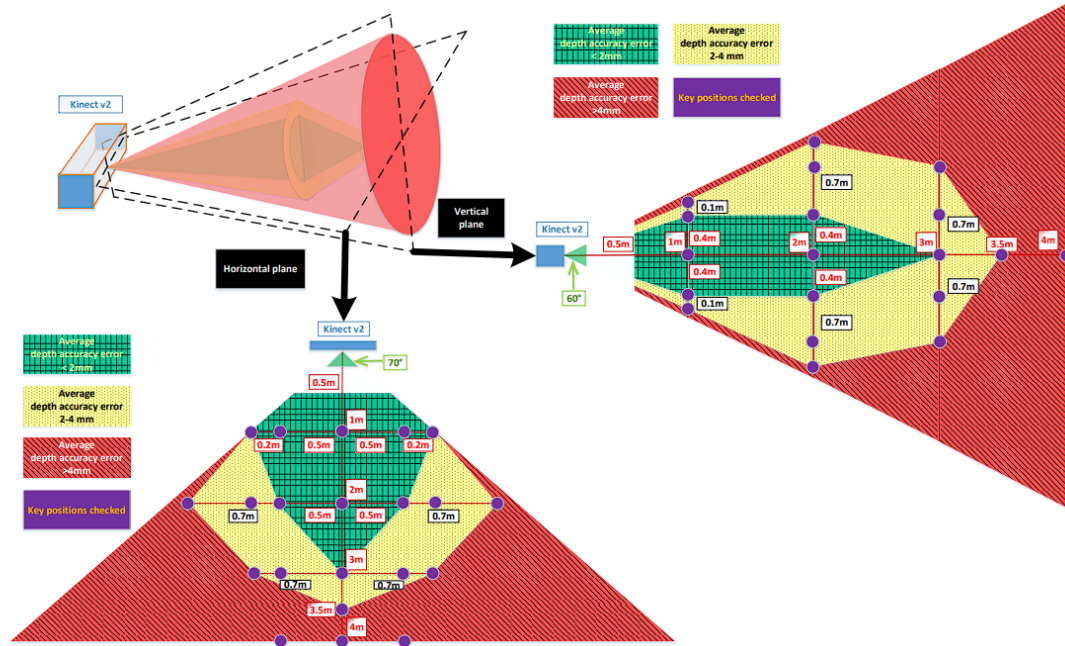


Figure 6 Depth Accuracy Error Distribution of Kinect V2 [16]

Figure 6 shows the average depth accuracy error in mm. An accuracy error less than 2mm is considered excellent, 2-4 mm considered not ideal and accuracy error greater than 4mm considered very poor. The diagram starts at a perpendicular distance greater than 0.5 m from the camera which is consistent with the manufacturer's specifications of a field of view (FOV) $70^\circ \times 60^\circ$ and an operating range from 0.5 to 4.5 m [20]. The diagram disagrees with the manufacturers' upper limit of 4.5 m, instead specifying a 3 m perpendicular distance from the camera as the ideal upper limit where depth information remains unobstructed. Any plyometric exercises performed in front of the Kinect sensor should be conducted within the safe green area to accurately capture depth and pose estimation data without added measurement noise.

2.2 Mild Traumatic Brain Injury and Persistent Long-Term Concussion Symptoms

More than three million Americans sustain a mild traumatic brain injury (mTBI) each year and 1 in 5 have persistent long-term symptoms beyond one month. "A traumatic brain injury occurs when an external force to the head or body alters brain function" [21]. While it is said that almost half of all Americans have sustained at least one TBI in their lifetime, the vast majority of TBIs (up to 90%) are classified as "mild". A mild TBI (mTBI) is characterized as a TBI that does not involve brief (< 30 min) loss of consciousness or any period of posttraumatic amnesia (<24h) [22]. Diagnosing mTBI poses challenges in various settings due to the subtle and transient nature of acute signs and symptoms associated with altered mental status. Additionally, commonly used diagnostic tests such as CT scans lack sensitivity. The complexity of diagnosis is further heightened in primary care settings, where patients are typically assessed days or even weeks after the injury event [21].

Concussions among varsity athletes are a particularly sensitive issue due to return to play pressures imposed by sport culture and poor return to play testing mechanisms [23]. It has been

shown that men's football, men and women's ice hockey and men's wrestling were the sports yielding the highest concussion incidence measures. Furthermore, concussion rates and risks are higher in females than in males [26]. Additionally, the ability to accurately diagnose concussions on the sidelines during active play has been shown to have its own issues due to athletes sandbagging their baseline testing [2]. It has been shown that athletes may intentionally provide sub-optimal effort in their baseline cognitive scores, and thus are able to return to play quicker than they otherwise would be allowed to if they provided optimal effort in their baseline test [24]. The computerized Immediate Post-concussion Assessment and Cognitive Test (ImPACT) is one of the sideline assessment tools which compares baseline and post-injury performance and is a common method used to aid in concussion diagnosis. The test has built-in validity indicators designed to flag results if they are suspected of "sandbagging". The manufacturer of ImPACT claims that their built-in validity indicators identify all but 11% of those attempting to sandbag. However, in a controlled study which randomized participants into a control group and a sandbagging group (control n = 37, sandbag n = 40), only 50% of the purposeful sandbag group were identified by current validity indicators [25]. Furthermore, successful sandbaggers were most likely to be first-time ImPACT test takers. The poor validity indicators of baseline concussion testing such as ImPACT underscore the need for a better, more objective way to test concussion symptoms on the sideline for return-to-play purposes for varsity athletes.

Patients recovering from concussion are prone to have Post-Concussion Syndrome (PCS). PCS is the persistence of concussion symptoms beyond the normal course of recovery of two weeks. When symptoms last longer than one or two months, doctors diagnose the patient with Post-Concussion Syndrome [27]. Persistent symptoms occur in 10-15% of patients [29]. PCS symptoms fall into four major categories: cognitive, sleep, mood/behavioral and physical. Many patients experience long term cognitive difficulties which keep them out of work or school for prolonged periods of time. Patients with cognitive difficulties are suggested to limit screen time during the first 48 hours after concussion, more specifically, in a study comparing recovery time for those who limited screen time vs those who did not, the group that limited screen time recovered to baseline in a median of 3.5 days (interquartile range, 2.0 > 10.0 days) while screen time-permitted group recovered in a median time of 8.0 days (IQR, 3.0 > 10.0 days, P = 0.03) [28]. In rare cases, cognitive issues can persist for a prolonged period of time for adolescents and is associated with poor academic and career outcomes due to significantly missed time at school. Poor sleep is common after concussion and clinicians suggest short term melatonin use improve sleep disturbance and reduce depressive symptoms in youth. Mood changes such as depression and anxiety are commonly experienced by patients after concussion. These symptoms may be related to physiological dysfunction due to the disturbance in the brain incurred by the concussion injury or simply due to stressors related to the injury circumstances [28].

Patients of TBI may experience vestibulo-ocular and vestibulo-spinal signs and symptoms. Vestibulo-ocular symptoms emerge when patients are moving their head in a static environment (walking or running) or are placed in a moving environment (riding in a car). In other words, the injured patient can be prone to dizziness and thus exhibit poor balance when moving in a static environment or in a moving environment after concussion. These impairments risk to not recover swiftly and often require direct treatment. If direct treatment is not completed in patients with balance impairments, the risk for long term post-concussion symptoms increases [30]. In an immediate concussion-focused neurological examination which focuses on neurological deficits through cranial nerves including visual fields, motor reflex and coordination examinations, the

most encountered abnormalities include cognitive function, vestibular function, gait and balance issues [30]. The Balance Error Scoring System (BESS) and the modified BESS are widely used validated tests which are typically used for diagnosing balance issues on the sideline for varsity athletes. The mBESS is a shortened version of the BESS which makes it more practical for use in a clinical and research settings. The standard BESS test typically includes three sensory conditions as shown in Figure 1 and the mBESS simplifies the testing conditions by including only two of the three sensory conditions [62]. Both tests use a scoring system based on the number of errors made by the individual during specific balance tasks. The BESS test is a powerful indicator for balance issues only within the first 4-5 days of concussion incidence since there is a high probability the injured athlete has returned to baseline within that time [30]. In a study of thirty-five collegiate student-athletes over a two year period with medically diagnosed sports-related concussions comparing the accuracy of the BESS and mBESS tests, it was recommended that the mBESS be used as a post-concussion balance assessment, despite limited efficacy measures [31].

Clinical researchers have been exploring alternative methods to the BESS and mBESS for assessing balance-related issues in athletes' post-concussion. The biomechanical performance during specific plyometric exercise has been assessed between individuals with concussion and healthy controls without concussion. In a cross-sectional study comparing 21 participants with sports-related concussion (age = 15.38 ± 1.77 years, height = 169.23 ± 8.59 cm, mass = 63.43 ± 7.39 kg) and 21 healthy controls (age = 15.36 ± 1.73 years, height = 169.92 ± 11.1 cm, mass = 65.62 ± 12.08 kg), it was found that athletes who returned to play within 30 days of concussion moved differently than healthy athletes [32]. In this study, participants performance was based on their performance of three double-limb jump-landing task by jumping off a 30 cm box onto force plates, the sequential motion described in Figure 7. The participants were recorded using a 3-dimensional motion-capture system (Qualysis AB) and two force plates.

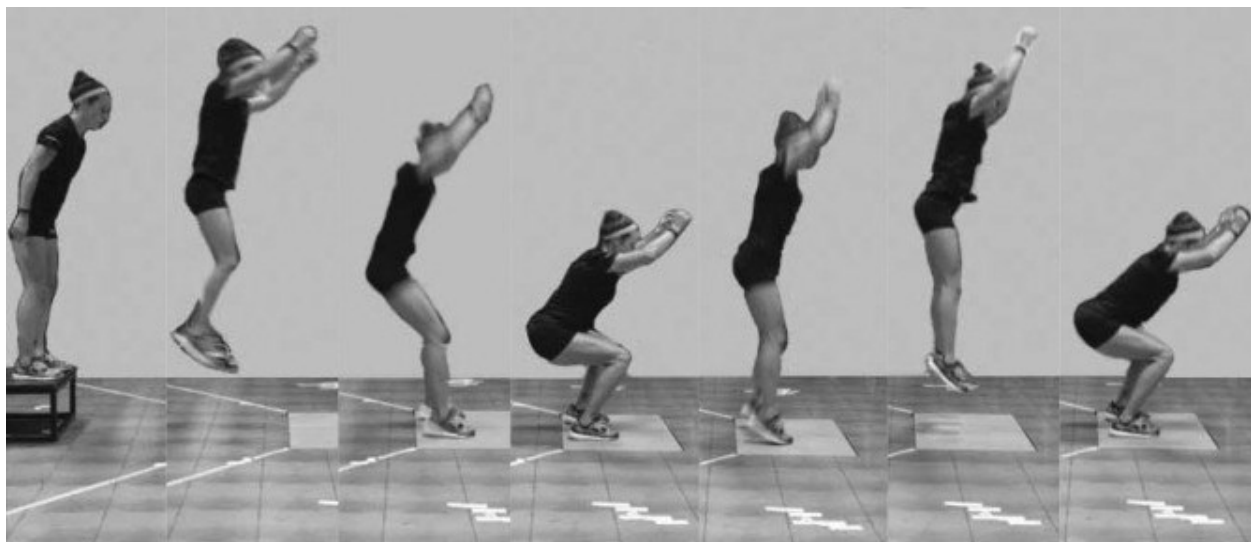


Figure 7 Double-Limb Jump Landing Sequential Motion [32]

The paper specifically compared their lower limb (dominant and non-dominant) knee variables including internal-varus moment (Nm/kg), extension moment (Nm/kg) and total sagittal-plane knee displacement (Degrees). The results of the study demonstrated that there were significant differences between the sports-related concussed and healthy control groups for all knee variables

on both the dominant and non-dominant limbs [32]. This investigation aligns with the research conducted by Lapointe et al., who investigated athletes with post-injury durations ranging from 0.9 to 6.5 years following a concussion. Their study revealed variations in knee kinematics subsequent to sports-related concussions. Notably, an elevation in knee abduction and internal rotation was identified during a jump-cut maneuver. Moreover, participants who experienced a concussion exhibited an augmented knee valgus at landing, particularly under unanticipated conditions as opposed to anticipated ones [33]. Dubose and colleagues noted alterations in single-limb drop-landing mechanics among athletes who experienced a concussion during a season when compared to their counterparts in the preceding season. This study consisted of Division I football players (13 concussed, 26 not concussed) and made use of a motion capture system in tandem with force plates to compute hip, knee and ankle joint stiffness. The results of the experiment demonstrated that those who suffered a concussion exhibited heightened hip stiffness and diminished knee and overall leg stiffness in comparison to athletes who did not encounter a concussion. It should be noted that this study concerned itself with those who were recently concussed with an average time from concussion to post-season testing of 49.9 days [34]. These studies suggest potential in examining pre-sports-related concussion movement patterns with post-injury patterns with pose estimation cameras in tandem with force plates.

Over the past decade, the methods employed in concussion rehabilitation have transitioned from a traditional approach involving 'rest and relaxation' to a more targeted focus on incorporating aerobic exercise [63]. In a randomized clinical trial evaluating the efficacy of aerobic exercise compared to a placebo-like stretching routine for individuals aged 13 to 18 years in the acute phase of sport-related concussion recovery (aerobic exercise $n = 52$; 24 female [46%]; stretching $n = 51$; 24 female [47%]), participants in the aerobic exercise group demonstrated a median recovery time of 13 days (interquartile range [IQR], 10-18.5), whereas those in the stretching group took 17 days to recover (IQR, 13-23) ($P = 0.009$ by Mann-Whitney test) [35]. The aerobic exercise group were instructed to perform aerobic exercise each day on a stationary bike or a treadmill, at home or in the gym at the prescribed target heart rate. The stretching group were instructed to follow a standard prescribed stretching program which is traditionally used for concussion patients on an "at rest" recovery program [35]. This study suggests an active rehabilitation program involving aerobic exercise is the more optimal approach in concussion recovery.

The strongest clinical predictor of a prolonged recovery is the patient's initial symptom severity in the first few hours after injury. Research has shown that initial rest (24-48 hours) with limited screen time following a concussion is recommended, however, prolonged rest has been linked to slower symptom resolution while exercise facilitates a quicker and more efficient recovery period [36]. However, clinicians note that aerobic exercise is not a "one size fits all" solution and each patient should be managed according to their clinical history.

2.3 Detecting Concussions and Balance with Pose Estimation Cameras & Force Plates

Researchers have suggested that balance issues may linger during plyometric exercises in the long term after recovering from a TBI [33], [34], [37]. There have been attempts to quantify the change in balance of recovered patients using force plates and pose estimation data. A pertinent paper which used force plates to measure the ground reaction forces (GRF) of patients instructed

to perform both a single leg hop and single leg squat, found that the time to stabilization (TTS) of the concussed group was longer than the control group for the single leg hop (mean difference = 0.35 seconds, confidence interval = 0.04, 0.64]; $F_{2,27} = 5.69$, $P = .02$) but no group differences were observed between control and concussed groups for the single leg squat [37]. The studies power included 30 college-aged recreational athletes (no varsity athletes included) and put into two groupings: a group of previously concussed individuals with a median time since concussion of 126 days (range = 28-432 days) and a control group of those who had no previous concussion history within 3 years of the study [37]. The study distinguishes between the dominant and non-dominant leg of the participant by asking them which leg they feel most comfortable kicking a soccer ball with. The participants were asked to perform five single leg hops and five single leg squats on each limb and data were averaged across all trials for a given limb [37]. Note that the in-depth descriptions of the mechanics of the single leg hop, single leg squat and drop vertical jump can be found in Chapter 3 of the thesis.

The time to stabilization metric is a way to calculate the total time participants take to establish almost perfectly stable balance during a plyometric exercise or dynamic balance stance [37], [59]. Time to stabilization can be computed by fitting the entire resultant ground reaction force from the trial with an unbounded third-order-polynomial and define the TTS as the moment when the unbounded third-order-polynomial force fit curve falls below what is known as the “normalized reference value” [37], [59]. By squaring each time-series value of the anterior-posterior (AP), medial-lateral (ML) and vertical (V) ground reaction forces, summing the values, and taking the square root of them, the resultant ground reaction force of each trial is obtained. The group mean and standard deviation of the control group were calculated and the “normalized reference value” is computed by adding three standard deviations to the mean range of variation and multiplying that by the respective participants body weight to compute the normalized reference value for each individual in both groups [37]. A time to stabilization value (in seconds) was computed for everyone in each group using the aforementioned methodology and an example of plotted results for the single leg hop are shown in Figure 8.

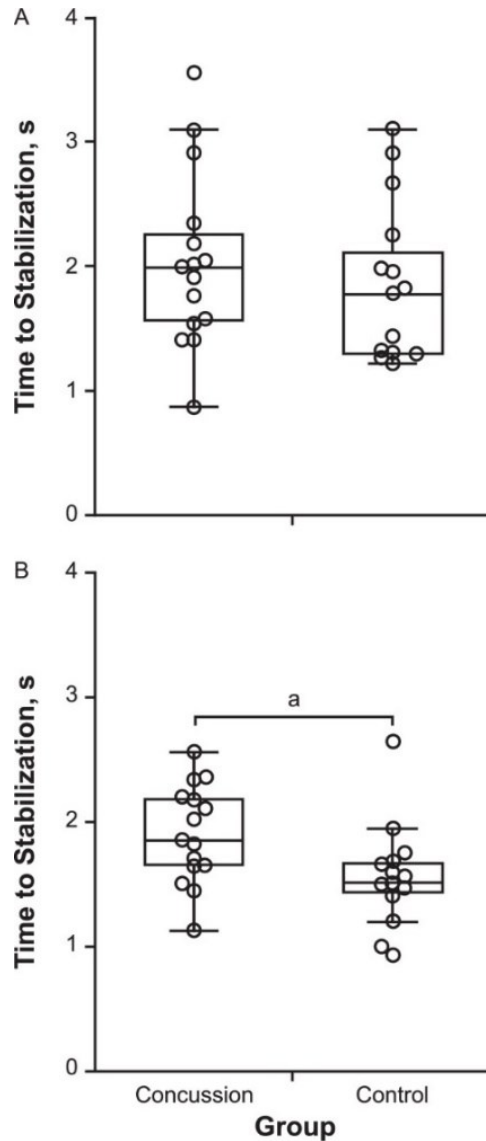


Figure 8 Time to stabilization during the single leg hop for both groups: A, on the dominant leg, and B, on the nondominant leg. a Indicates a between-groups difference ($F_{2,27} = 5.69$, $P = .02$) [37].

The musculoskeletal GaitFullBody model is based on the AnyBody modelling software which is a proprietary software created by AnyBody Technology which allows users to create detailed full body musculoskeletal models to simulate internal body loads and joint reaction forces [40]. The model works by intelligently superimposing the Kinect V2's key points onto the required Key points for the AnyBody modelling system shown by the green dots in Figure 9. "This was achieved by solving a non-linear least-square optimization problem to minimize the least-square difference between the virtual markers on the stick figure and those on the musculoskeletal model" [39]. This methodology ensures that the musculoskeletal model is directly driven by the pose estimation data obtained from the Kinect V2. The ground reaction forces are then computed by introducing muscle-like actuators at 25 contact points under each foot (shown in Figure 9 (B)). Ground contact

was defined when the foot nodes were sufficiently close to the ground (50 mm) and the normal force imposed to the floor was computed. The mediolateral and anteroposterior ground reaction forces were then easily computed by using an assumed friction coefficient of 0.1 [41].

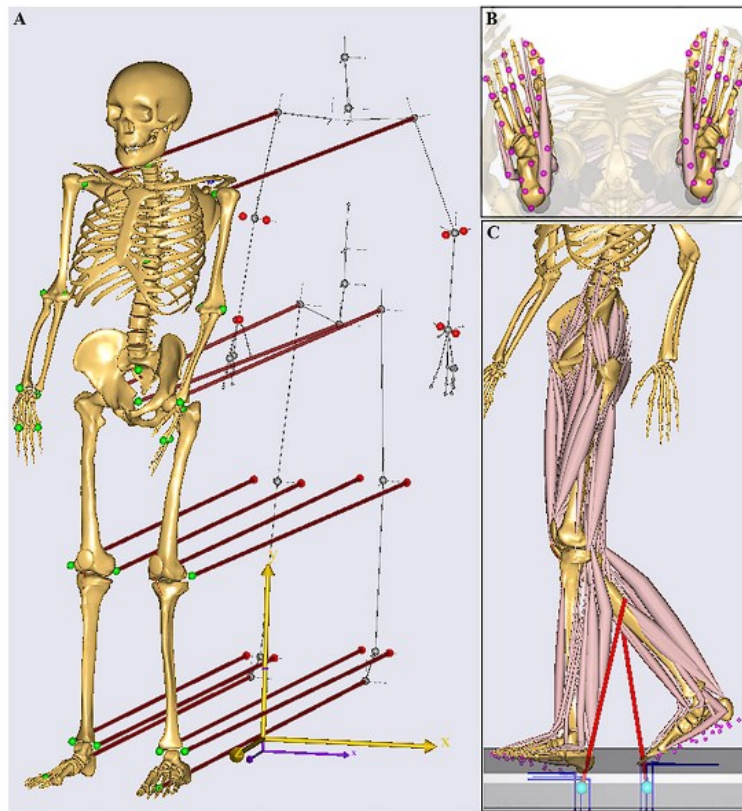


Figure 9 (A) The Kinect-Driven musculoskeletal model, (B) 25 contact points under the foot, (C) musculoskeletal model working during one gait trial with calculated GRF [39].

The results of the calculated ground reaction force in all three directions from developed model were compared to the measured ground reaction forces using standard force plates and the results are shown in Figure 10.

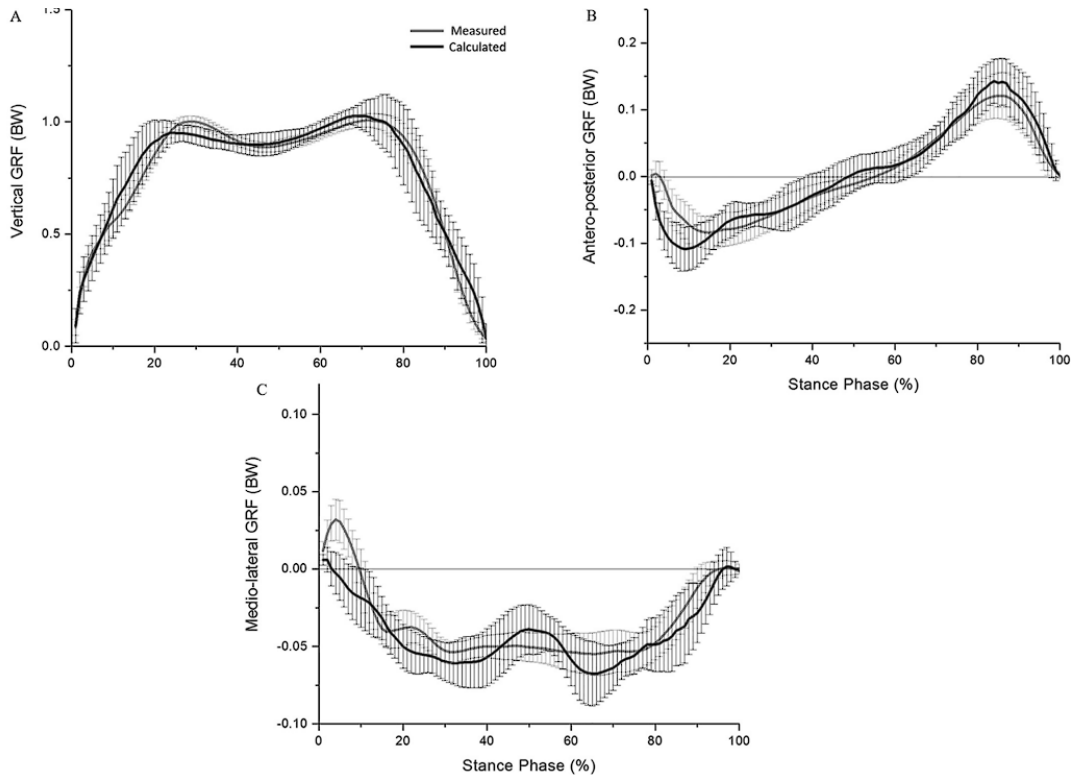


Figure 10 Ensemble curves (mean and 90% confidence intervals) of the measured vs calculated GRF in all directions [39].

The results demonstrated in Figure 10 are taken from initial contact to toe-off portion of the jump and clearly demonstrate a strong correlation between measured and calculated ground reaction forces in all three directions. More specifically, the vertical and antero-posterior GRF show the strongest correlation between measured and unmeasured whereas the medio-lateral GRF shows less correlation but still acceptable for most stance phases. These results demonstrate the possibility and strong potential of using pose estimation cameras to estimate ground reaction forces and thus retrieve accurate time to stabilization balance metrics to evaluate concussions.

Additional studies evaluating balance using pose estimation cameras have successful results. A study examining whether pose estimation metrics paired with SVM classification models can classify gait differences in probands (PB) and typically developing siblings (TD), demonstrated that pose estimation metrics can correctly distinguish between PB and TD [42]. This was accomplished by analyzing known metrics used for gait synchrony such as the variance of the swinging frequencies of each child's arms using the Fast Fourier Transform (FFT), denoted as $\sigma_f^2 max$. The smaller the value of the variance, the more synchronous the limbs were. Another example of a metric they used was the variance of the angle between the vertical axis and the line connecting the neck and torso, denoted as $\sigma_{\theta_5}^2$ [42]. $\sigma_{\theta_5}^2$ was the most statistically significant metric out of all the ones used for both boys and girls when identifying group differences between PB and TB and could show promise as a metric used for other aerobic exercises besides traditional gait analysis [42]. Using the aforementioned metrics in tandem with four more gait-based metrics to determine balance, an SVM classifier showed promising results in classifying PB and TB,

showing precision of 0.86, recall of 0.80, specificity of 0.45 and F1 score of 0.83 in a relatively symmetrical dataset (n = 15 PB, 12 TD) [42].

Total body centre of mass (TBCM) is a traditionally useful kinematic measurement of body sway used for assessing postural stability, however, it requires expensive equipment and high technical requirement [43]. A study evaluating if the Kinect V2 camera can accurately quantify the TBCM proved the Kinect produced highly correlated measurement of TBCM sway (mean RMSE = 4.38 mm; mean CORR = 0.94) compared to the industry gold-standard Vicon and force plates [43]. The TBCM coordinates are computed as a simple weighted sum of center of mass (CM) coordinates of each body part:

$$x_{TBCM} = \frac{\sum_{i=1}^{15} m_i x_{i,CM}}{M} \quad (1)$$

$$y_{TBCM} = \frac{\sum_{i=1}^{15} m_i y_{i,CM}}{M} \quad (2)$$

Where x_{TBCM} and y_{TBCM} are the coordinates of the TBCM, $x_{i,CM}$ and $y_{i,CM}$ are coordinates of the i-th segment, m_i is the mass of the i-th segment and M is the total body mass of the 15 body segment model [43]. Each body segment center of mass coordinates is computed using the coordinates of the proximal and distal ends of the respective segments and the percentage of segmental length from the proximal and distal ends respectively. The aforementioned variables are defined by Dempster's body segment parameters [44]. The following equations define the center of mass for the i-th body segment:

$$x_{i,CM} = x_p l_p + x_d l_d \quad (3)$$

$$y_{i,CM} = y_p l_p + y_d l_d \quad (4)$$

Where $x_{i,CM}$, $y_{i,CM}$ are the coordinates of the CM; x_p and y_p are coordinates of the proximal end, x_d and y_d are coordinates of the distal end and l_p , l_d are the percentage of segmental length from the proximal and distal ends [43]. The results of their experiment demonstrated that although the Kinect consistently overestimated 95% confidence intervals of TCBM displacement, the results of RMSE and CORR showed that TBCM trajectories of the Kinect mostly agree with the Vicon camera and force plate data. In fact, the Kinect sometimes performed better than the force plate data for more complicated balance tasks [43]. This methodology of computing the TCBM trajectory for balance evaluation may prove valuable in the study of assessing a history of concussion in varsity athletes using a Kinect V2 camera.

Using similar methodology as defined in [43] for computing TBCM using centre of mass of each segment, a paper studying nine healthy individuals completing three standing balances: double limb stance with feet apart, double limb stance with feet together and a single limb stance found that the Kinect V2 is a valid, reliable and convenient device for assessing standing balance [45]. More specifically, the paper found strong correlation between the Kinect System and

Optotrak Certus motion capture system when comparing centre of mass position variability and average velocity of centre of mass in the horizontal plane [45].

2.4 Classical Machine Learning Techniques

There are many classical machine learning techniques used throughout the course of the research. Machine learning encompasses different main tasks such as regression, feature selection and logistic regression (classification). Logistic regression, or more widely referred to as “classification” involves assigning labels to objects in a dataset [46]. This section presents a brief literature review of the different algorithms used in the data analysis portion of the research. The most commonly used machine learning algorithms used throughout the course of research were different classifiers such as support vector machines (SVM), K-Nearest Neighbors (KNN), multi-layer perception (MLP) and decision trees. In addition, multiple regression algorithms used for ground reaction force estimation were explored throughout the research.

Multi-Layer Perceptron (MLP):

“A multi-layer perceptron is a type of neural network consisting of multiple layers of neurons” [47]. The MLP is the most popular feedforward neural network and is widely used to tackle different classification and prediction problems [48]. A neural network is made up of interconnected nodes, known as neurons, arranged in layers. Each neuron takes in input signals, processes them using an activation function, and generates an output signal, which can be transmitted to other neurons in the network. The activation function determines a neuron's output based on its input, introducing nonlinearity into the network, and allowing it to learn complex data patterns [47]. Figure 11 shows the common architecture of an MLP.

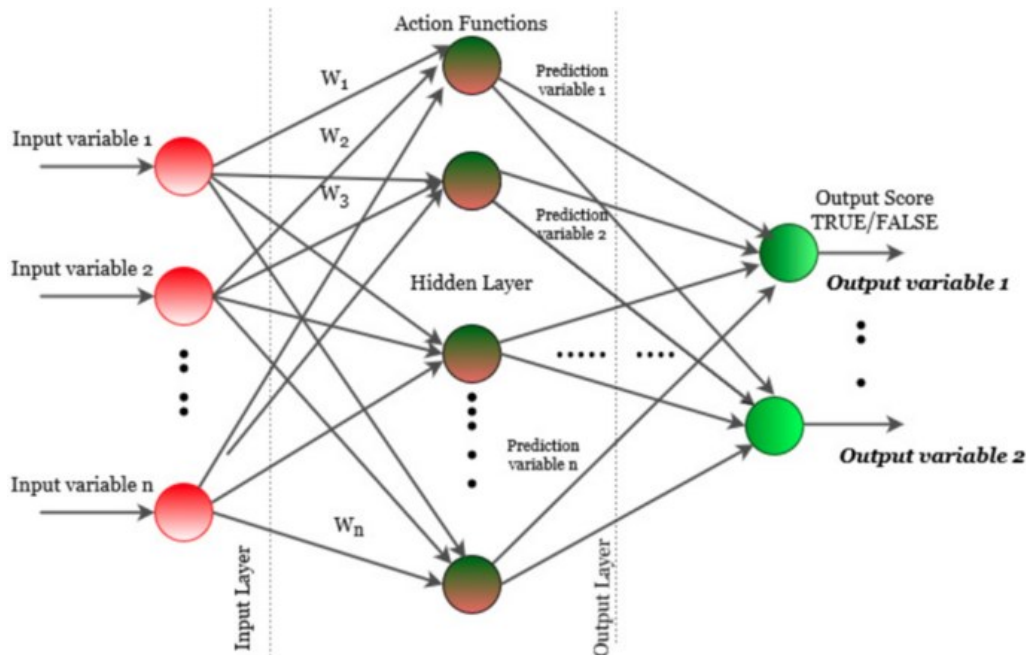


Figure 11 Typical Architecture of an MLP [49]

The MLP algorithm is an iterative machine learning algorithm which uses the error signals to update the weights fed into the hidden layer until converging to a target output. The algorithm

starts off by randomly choosing initial weights and multiplying those weights by the inputs to the network and adding a bias term. Afterwards, the algorithm applies the selected (usually non-linear) activation function then computes the output for every neuron from the input layer. The algorithm then computes the output error using a loss function. Loss functions include mean-squared error, mean absolute error for the regression tasks and cross-entropy loss, categorical cross entropy loss for the classification task (binary or multiclass classification). After computing the error given the selected loss function pertinent to the machine learning task being performed, the algorithm makes use of gradient descent to adjust the weights. The algorithm then applies the weight adjustments and repeats the mentioned steps until converging with the target output [49].

Support Vector Machines (SVM):

Support vector machines are one of the most powerful supervised machine learning techniques- a robust classification and regression strategy. The goal of all classification algorithms is to define boundaries in the multi-dimensional parameter space for classifying several unique datapoints [50]. The decision boundary in SVMs is decided by maximizing the margin between the decision space using what are known as support vectors. A notable advantage of SVM over other classification strategies is its ability to employ a limited number of support vectors in comparison to the size of the input data which allows for quicker convergence [50]. The two-dimensional example of a maximum margin SVM classification strategy is shown in Figure 12 below.

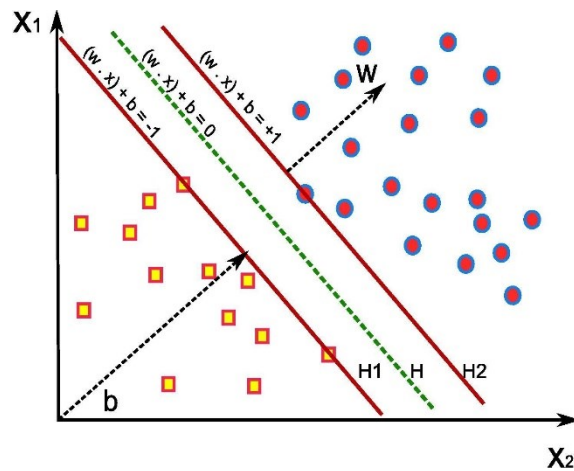


Figure 12 Two-Dimensional Example of SVM Maximum Margin Classifier (boundary = green line) [50]

K-Nearest Neighbors (KNN):

K-Nearest Neighbors is a simple, yet effective supervised learning algorithm primarily used for classification. The working assumption of KNN is that similar data points can be found near one another [51]. The KNN algorithm will hold all of the training data and their known labels in memory whenever a new, never-before-seen data point enters the fold. When a new unlabeled data point is encountered in the dataset, KNN performs two operations: firstly, it analyzes the *K* points closest to the new data (*K* is a hyperparameter which may be tuned by the programmer), secondly, using the neighbour's classes, KNN determines which class the new data point belongs to by means of simple majority vote [52]. There are multiple different distance metrics a KNN algorithm

may use in order to quantify the space between the query point and the other data points such as Euclidean distance, Manhattan distance, Minkowski distance and hamming distance [51]. The hyperparameter K in K Nearest Neighbors defines how many neighboring points the new query point will be compared to. The most optimal choice for the value K is dependent on the data and is accomplished by employing a validation set and performing a grid search for different K values. The K value that returns the best accuracy is the chosen value for K for the specific dataset [52].

Decision Trees:

Decision trees are a machine learning model used for both classification and regression. The working principle of decision trees is a model which answers typical questions of the form “if this than that” [53]. An example of a basic decision tree used for whether or not to play golf on a given day is shown in Figure 13. The tree works by starting at the top and working its way downward until it reaches a final result of whether or not to play golf. This example can be extended to many more complicated tasks like assessing whether a patient has lung cancer given a cornucopia of patient information or detecting concussion history in athletes using many metrics obtained from pose estimation data.

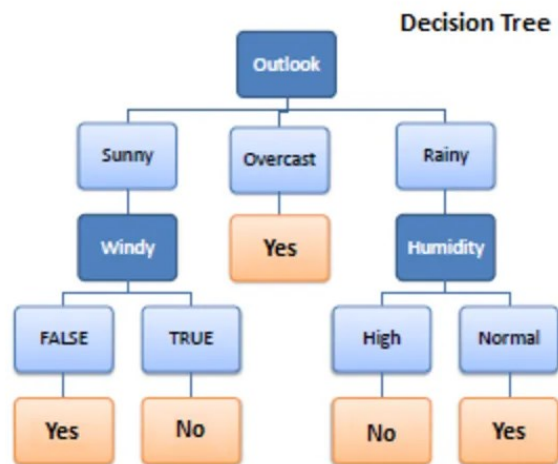


Figure 13 Simple Example of Decision Tree used for Deciding whether to play Golf [53]

The decision tree model has great potential in applications of medical research since results are easy to understand and interpret, robust to outliers and easily handles heavily skewed data without resorting to data transformation. However, one needs to adequately balance the complexity and robustness of a decision tree model. For example, an overly complex decision tree model risks overfitting the data by creating a model that spreads wide enough to make all records in each leaf node have the same target outcome. To prevent this from happening, stopping rules must be implemented to prevent a decision tree model from becoming too complex. In situations where stopping conditions do not work, an alternative known as “pruning” which involves reducing the size of a complex tree by removing non-significant branches through use of a chi-squared test or multiple-comparison adjustment methods [54]. A random forest decision tree is a type of decision tree which combines the output of multiple decision trees to reach a single result. The random forest decision tree generates a random subset of features which ensures low correlation among decision trees which reduces overfitting, bias and overall variance [66].

Regression Models:

The main goal of the classification task is to predict the category or class to which a new data point belongs to whereas regression aims to predict a continuous numerical value or quantity based on training data. There are many regression algorithms such as linear regression, decision trees for regression, neural networks, random forest regression, etc. Standard linear regression works by creating an objective error function and attempting to drive the error to zero by updating the parameters through gradient descent [55]. Many different objective functions may be used such as the Mean Squared Error (MSE), Mean Absolute Error (MAE), R-Squared, etc. The gradient of the objective function is computed and represents the magnitude and direction the parameters must be updated to and scaled by a learning rate α which must be tuned by the programmer as too high a learning rate may lead to no convergence and too low a learning rate may lead to convergence which is extremely slow. The regression algorithm runs iteratively until the updated parameters of the model do not change significantly for multiple iterations in a row [56].

Chapter 3 Data Description & Methodology

The dataset is comprised of 444 varsity athletes (36.26% Female) from the 2022 cohort and 464 athletes (38.76% Female) from the 2023 cohort from McGill and Concordia University located in Montreal, Quebec, Canada. The athletes come from varied sports background including basketball, cross country, football, hockey, lacrosse, rugby, soccer, swimming, track and field and volleyball. The percentage sport split of varsity athletes for the 2022 and 2023 cohorts are shown in Figure 14 and Figure 15, respectively.

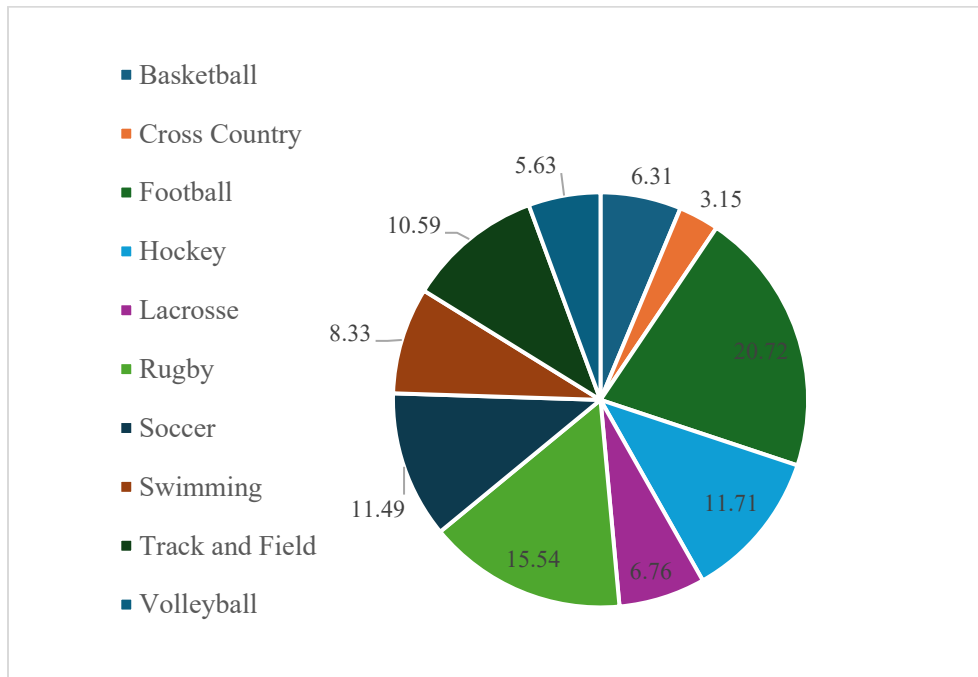


Figure 14 % Split of Varsity Sport for All Athletes - 2022 Data (N = 444)

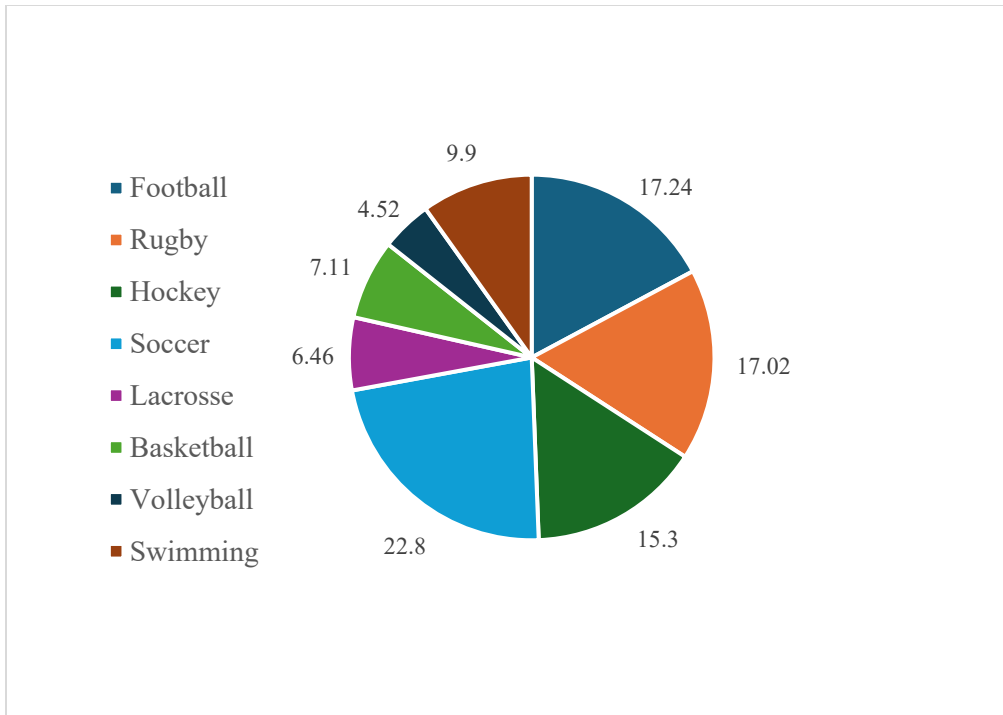


Figure 15 % Split of Varsity Sport of All Athletes - 2023 Data (N = 464)

3.1 Description of Performed Exercises

The athletes performed multiple drop vertical jumps, single leg squats and single leg hops during their pre-season physicals in addition to filling out a questionnaire about their concussion history in both the 2022 and 2023 years. The study was conducted in accordance with ethical guidelines and received approval from the Institutional Review Board (IRB) at McGill University. Written consent was obtained from all participants.

Drop Vertical Jump:

The drop vertical jump is a popular plyometric exercise which involves an athlete dropping off a stationary platform (height = 31cm), landing on both feet and immediately performing a maximal vertical jump and landing again [57]. Every athlete in both 2022 and 2023 performed at least three DVJ's each. Figure 16 shows the pose estimation sequence of motion for a typical drop vertical jump performed within our cohort. Each athlete performed around three drop vertical jumps in both 2022 and 2023.

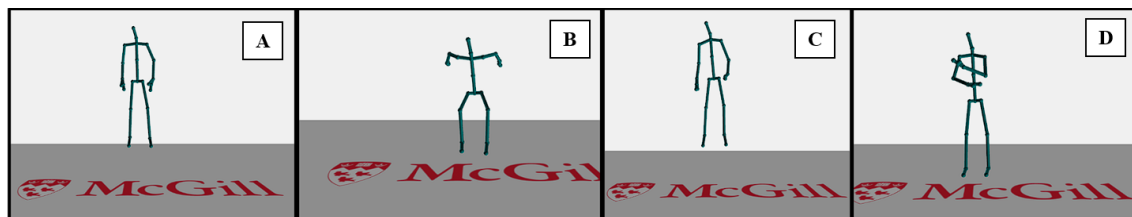


Figure 16 Sequence of motion of DVJ. (A) Initial Resting Position, (B) First Landing, (C) Maximal Vertical Jump, (D) Second Landing

Single Leg Squat:

The single leg squat, sometimes referred to as a pistol squat, is a squat movement which is performed on one leg (either the dominant leg or non-dominant leg). The single leg squat is meant to test balance and stability. Each athlete from the 2023 cohort recorded six single leg squats (three on their left leg, three on their right leg) whereas only a few athletes recorded single leg squats in the 2022 data cohort. Note that each athlete performs two single leg squats per recording (to distinguish the two jumps, their metrics are prefixed with “First” and “Second” in the dataset). Figure 17 shows the sequence of motion for a typical single leg squat.

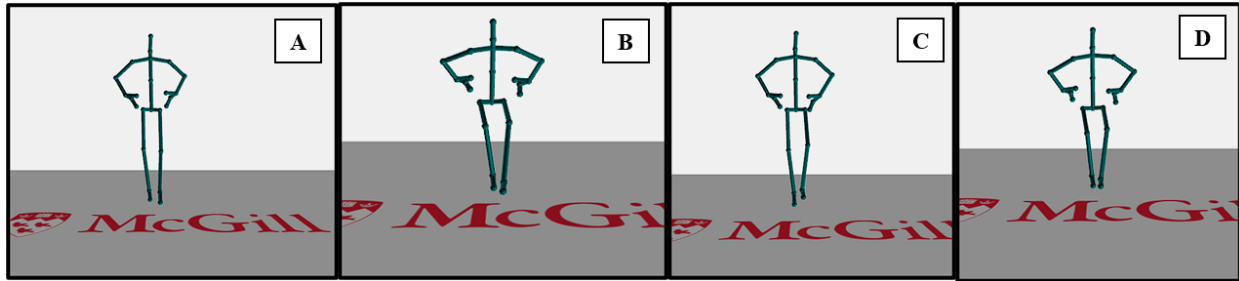


Figure 17 Sequence of Motion of SLS: (A) First One Leg Standing Position, (B) First Squat Full Flexion, (C) Second One Leg Standing Position, (D) Second Squat Full Flexion

It is important to note that it was qualitatively reported that there is high variance to the degree in how far an athlete squats downwards. In other words, some athletes would not squat very far down, some would squat to the suggested height, and some would squat much further than directed by our research team.

Single Leg Hop (SLH):

The single leg hop exercise is a plyometric drill which helps athletes develop power in their legs along with improving balance and stability. To perform a single leg hop, the athlete starts standing on one leg, subsequently loads up their supporting leg into a forward jump and finishes off by landing on their supporting leg until returning to balance equilibrium. Nearly every athlete in the 2022 cohort completed six single leg hops (three on their left leg, three on their right leg) whereas only a few athletes recorded single leg hops in the 2023 cohort. Figure 18 shows the sequence of motion for a typical single leg hop.

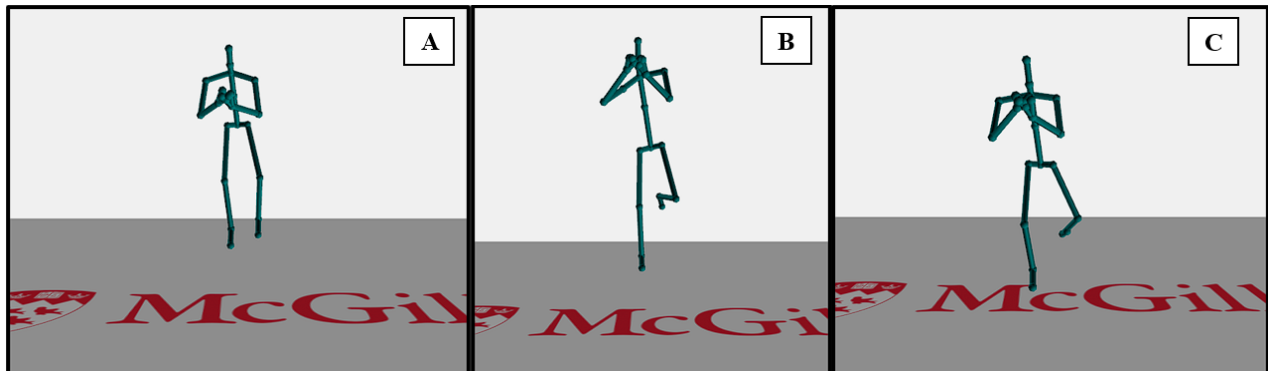


Figure 18 Sequence of Motion for a SLH. (A) Initial Single Leg Balancing Position, (B) Forward Jump Phase, (C) Landing Phase

3.2 Comparing 2022 and 2023 Datasets

The 2022 and 2023 cohorts contain a breadth of concussion history information. However, the 2023 cohort contains a greater depth of information due to the inclusion of a revised concussion questionnaire that was put together given professional advice from concussion specialists. Both datasets contain patient information including first name, last name, sex, age, height, weight, varsity sport and a unique identifier. Moreover, both datasets contain information about each patient’s knee pain, previous lower limb injuries, physical health status, smoker status, contraceptives used (if applicable), if they sustained an anterior cruciate ligament (ACL) injury and on which leg. The concussion information in 2022 is limited to number of diagnosed concussions and year each concussion was sustained whereas the 2023 dataset contains number of diagnosed concussions, number of suspected undiagnosed concussions, age/month/year of each diagnosed concussion, a list of concussion symptoms and the concussion recovery time.

The 2022 cohort contains 444 varsity athletes with a total of 153 of them having a history of one or many diagnosed concussion(s). The 2023 cohort contains 464 varsity athletes with a total of 168 of them having a history of diagnosed concussion(s) and 211 of them having a history of at least either a suspected undiagnosed concussion or a diagnosed concussion. We have 127 common athletes that were a part of both the 2022 and 2023 cohorts. Of the 127 common athletes in both years, 119 of them (33.6% Female) performed the drop vertical jump in both 2022 and 2023. On average, each of these common athletes performed three drop vertical jumps each in both 2022 and 2023. The varsity sport percentage split along with the average weight, height and age of each cohort can be found in Table 1 and Table 2 for 2022 and 2023, respectively.

Table 1 2022 Varsity Sport % Split and per-sport Average Weight (kg), Average Height (m) and Average Age

Sport	% of Cohort	% of Concussed	Average Weight (kg)	Average Height (m)	Average Age
Basketball	6.31	3.92	82.85	1.86	21.10
Cross Country	3.15	1.31	64.44	1.75	20.14
Football	20.72	22.22	96.23	1.83	21.67
Hockey	11.71	16.99	78.05	1.76	21.11
Lacrosse	6.76	7.84	81.84	1.81	19.33
Rugby	15.54	18.30	78.33	1.74	21.02
Soccer	11.49	9.80	68.89	1.74	19.85
Swimming	8.33	4.58	70.03	1.75	19.78
Track and Field	10.59	8.50	69.365	1.75	19.86
Volleyball	5.63	6.54	70.85	1.78	20.64

Table 2 2023 Varsity Sport % Split and per-sport Average Weight (kg), Average Height (m) and Average Age

Sport	% of Cohort	% of Concussed Athletes	Average Weight (kg)	Average Height (m)	Average Age
Basketball	7.1	6.63	78.37	1.83	20.8
Football	17.2	19.9	93.25	1.82	21.5
Hockey	15.3	19.4	78.5	1.76	21.58
Lacrosse	6.5	8.05	82.2	1.8	20.3
Rugby	17.0	19.9	84.19	1.78	20.4
Soccer	22.8	18	69.26	1.72	20.6
Swimming	9.9	2.84	66.98	1.73	20.5
Volleyball	4.5	5.2	73.87	1.78	22.09

3.3 Data Capture and Processing Methodology

Athletes performed the drop vertical jump; single leg squat and single leg hop during their pre-season physicals in front of the Kinect V2 camera (software SDK version 2.0) which was centered and placed 2.5 metres away from the subject. Throughout each participant's exercise session, KITS records and stores both time-series joint and estimated ground reaction force data. Utilizing this time-series data, KITS calculates various exercise-specific metrics, all of which will be detailed in the following section. It should be noted the joint position names listed in all equations correspond to the Kinect V2 joint positions published by Microsoft Studios [58].

3.3.1 Time-Series Joint Information

There are two main angles captured below the torso of the athlete's body which are the coronal and sagittal angles depicted in Figure 19. The variables $KneePositionX$ and $AnklePositionX$ represent the X coordinates of the 3D positions of the knee and ankle, respectively. Additionally, \overrightarrow{femur} and \overrightarrow{tibia} denote vectors originating from the knee positions towards the hip joint and ankle positions, respectively.

$$\theta_{\text{coronal}} = \sin^{-1} \left(\frac{KneePositionX - AnklePositionX}{\|\overrightarrow{tibia}\|} \right) \quad (5)$$

$$\theta_{\text{sagittal}} = 180^\circ - \cos^{-1} \left(\frac{\overrightarrow{femur} * \overrightarrow{tibia}}{\|\overrightarrow{femur}\| * \|\overrightarrow{tibia}\|} \right) \quad (6)$$

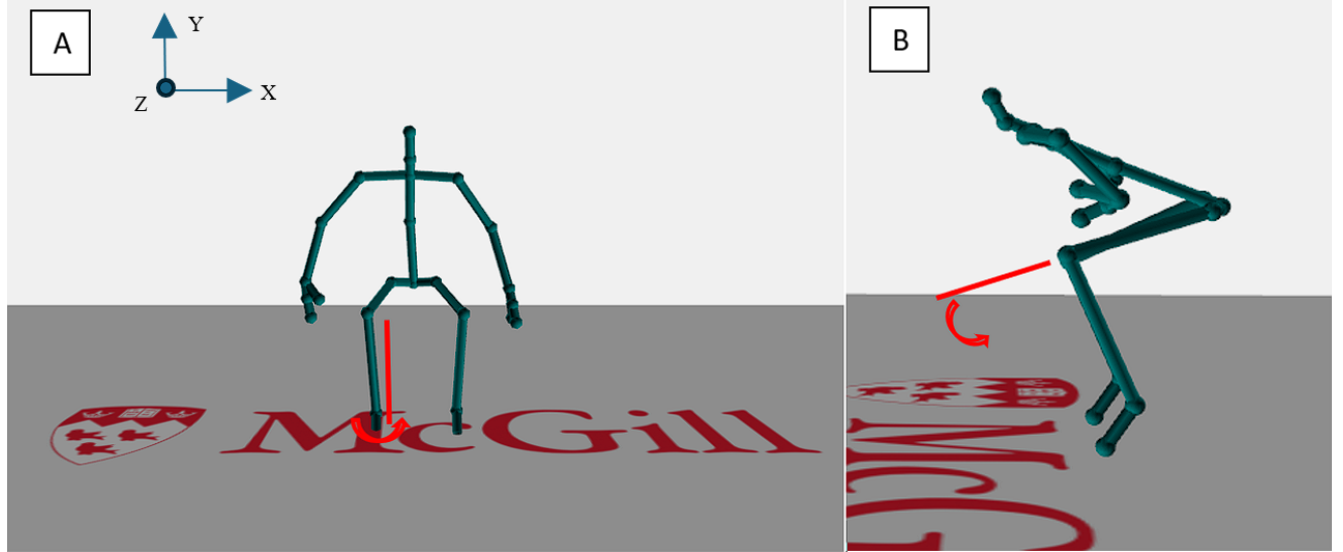


Figure 19 (A) Coronal Knee Angle and (B) Sagittal Knee Angle

There are four recorded angles from the pelvis to just before the neck: spine sway X, spine sway Z, pelvis tilt Y, pelvis tilt Z. Figure 20 shows the angles in action. The variables $SpineShoulderX$, $SpineShoulderZ$, $SpineBaseX$, $SpineBaseZ$ represent the X and Z coordinates of the joints at the top and bottom of the spinal column, respectively. $LeftHipY$, $LeftHipZ$, $RightHipY$ and $RightHipZ$ represent the Y and Z coordinates of the joints at the left and right side of the athlete's hip, respectively. \overrightarrow{spine} is a vector created from the $SpineShoulder$ and $SpineBase$ joints whereas the \overrightarrow{hip} is a vector created from the $LeftHip$ and $RightHip$ joints.

$$\theta_{SpineSwayX} = \cos^{-1}\left(\frac{SpineShoulderX - SpineBaseX}{\|\overrightarrow{spine}\|}\right) - 90^\circ \quad (7)$$

$$\theta_{SpineSwayZ} = \cos^{-1}\left(\frac{SpineShoulderZ - SpineBaseZ}{\|\overrightarrow{spine}\|}\right) - 90^\circ \quad (8)$$

$$\theta_{PelvisTiltY} = \cos^{-1}\left(\frac{LeftHipY - RightHipY}{\|\overrightarrow{hip}\|}\right) - 90^\circ \quad (9)$$

$$\theta_{PelvisTiltZ} = \cos^{-1}\left(\frac{LeftHipZ - RightHipZ}{\|\overrightarrow{hip}\|}\right) - 90^\circ \quad (10)$$

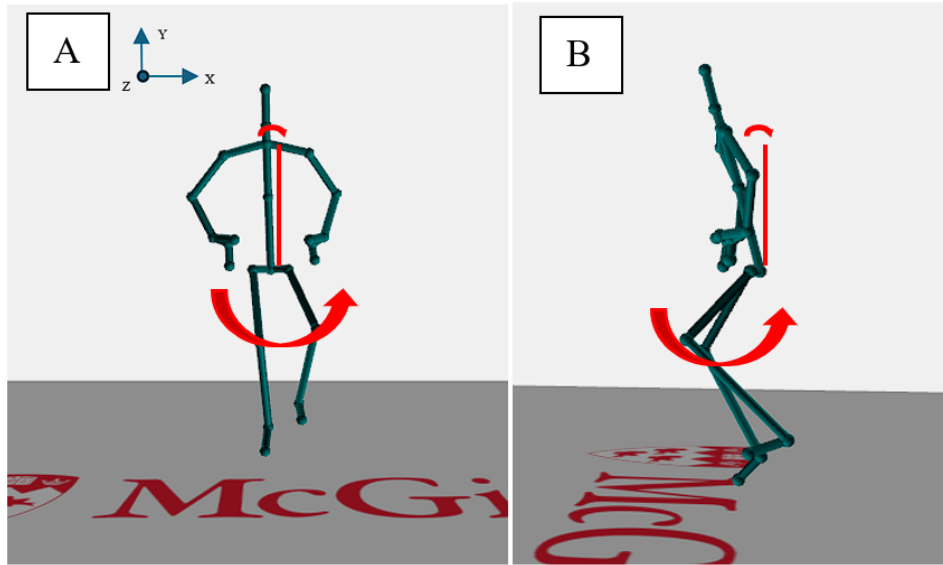


Figure 20 (A) Spine Sway X shown by angle between vertical line and spine, Pelvis Tilt Y shown by large sweeping arrow, (B) Spine Sway Z shown by angle between vertical line and spine, Pelvis Tilt Z shown by large sweeping arrow.

There are four remaining statistics that are computed which pertain to the neck, wrists, and ankles: neck sway X, neck sway Z, wrist distance and ankle distance. These measures are shown in Figure 21. The $HeadX$, $HeadZ$, $NeckX$ and $NeckZ$ are the X and Z joint positions of the head and neck, respectively. \overrightarrow{Neck} is a vector created from the head and neck joint positions. $LeftWristCoords$ and $RightWristCoords$ are the 3D coordinates of the left and right wrists. $LeftAnkleCoords$ and $RightAnkleCoords$ are the 3D coordinates of the left and right ankles.

$$\theta_{NeckSwayX} = \cos^{-1}\left(\frac{HeadX - NeckX}{\|\overrightarrow{Neck}\|}\right) - 90^\circ \quad (11)$$

$$\theta_{NeckSwayZ} = \cos^{-1}\left(\frac{HeadZ - NeckZ}{\|\overrightarrow{Neck}\|}\right) - 90^\circ \quad (12)$$

$$D_{Wrist} = \|\overrightarrow{LeftWristCoords - RightWristCoords}\| \quad (13)$$

$$D_{Ankle} = \|\overrightarrow{LeftAnkleCoords - RightAnkleCoords}\| \quad (14)$$

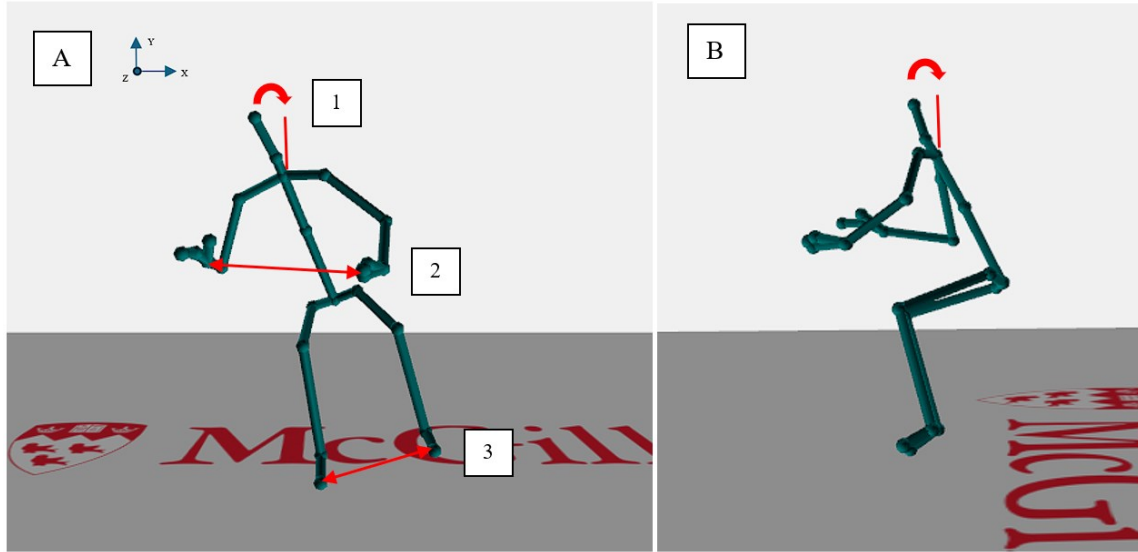


Figure 21 (A.1) Neck Sway X, (A.2) Wrist Distance, (A.3) Ankle Distance and (B) Neck Sway Z

3.3.2 Time-Series Ground Reaction Forces

In addition to the standard body angles computed by our KITS pose estimation software, we created a random forest decision tree regression model to predict ground reaction forces in the vertical, medial-lateral, and anterior-posterior directions throughout time. This was made possible by utilizing data obtained from an additional experiment carried out by our research team which involved 40 test subjects performing three drop vertical jumps, six single legged squats (three on each leg) and six single legged hops (three on each leg) each. The test subjects' motion was recorded using a Kinect V2 and their ground reaction forces along with their center of pressure (COP) was recorded using a set of force plates from Advanced Mechanical Technology Inc. (Watertown, USA) model BP400600-2000 with a refresh rate of 2000 Hz. The Kinect V2 and force plate recordings were synchronized when the patient began the respective exercise. Our software contains event indicators throughout each exercise including the recorded frames of initial contact and toe-off for the drop vertical jump and single legged hop. These recorded events were used to synchronize force plate and Kinect data along with appropriate down sampling of the force plate data to match Kinect V2 refresh rate of 30 frames per second. The single legged squat data processing only required down sampling force plate data to match the Kinect refresh rate. No attention was paid to event kick-offs for the single legged squat since the subject is in constant contact with the force plate for the entire length of the exercise unlike the drop vertical and single leg jumps where the subject is in the air for a portion of the exercise.

After pre-processing the data for the three exercises, several regression models were tested as prospects to accomplish accurate ground reaction force predictions. Minimization of the root mean squared error was a strong factor when considering which model to choose but the ability for the model to follow the trend of the actual force was of utmost importance due to its role in computing time to stabilization which is further explained in section 3.3.5. BMI, left & right coronal angle, left & right sagittal angle and spine sway in the X direction were the features used as predictors. Additional predictors such as pelvis tilt Y & Z, wrist distance, or ankle distance proved to not increase accuracy of the models. It is important to note that the patient's weight was subtracted out of the vertical ground reaction force during training and added back in test to achieve

standardization. This method proved to significantly increase the model’s performance. Figure 22 shows six different regression models which were tested on the same test sample of the second landing phase of a drop vertical jump. Figure 23 shows six different regression models tested on the same test sample for the recorded first squat of the SLS exercise.

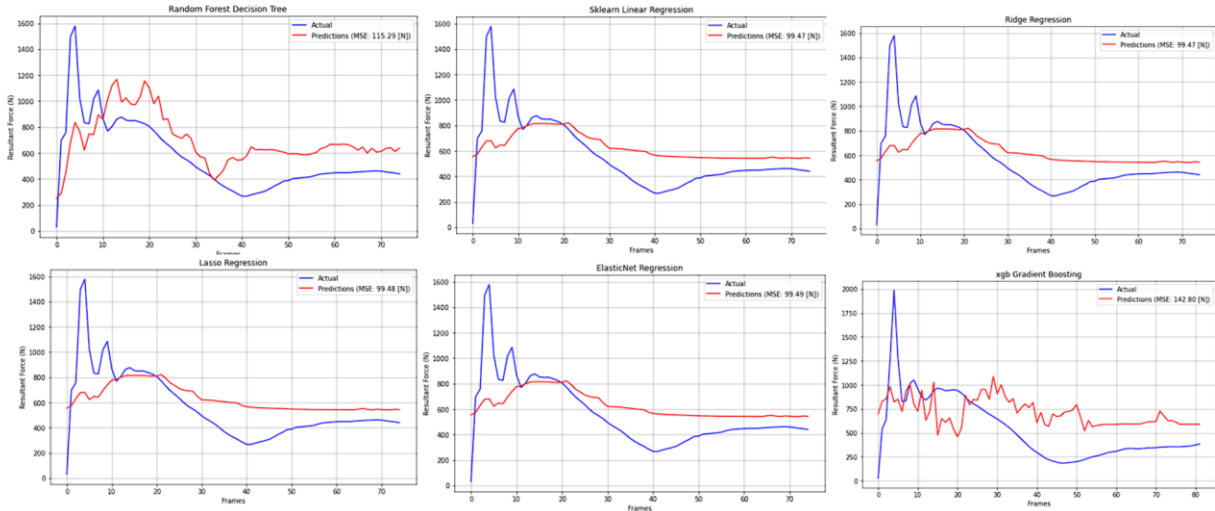


Figure 22 Actual vs Predicted Ground Reaction Forces using six different regression models for the second landing of the DVJ.

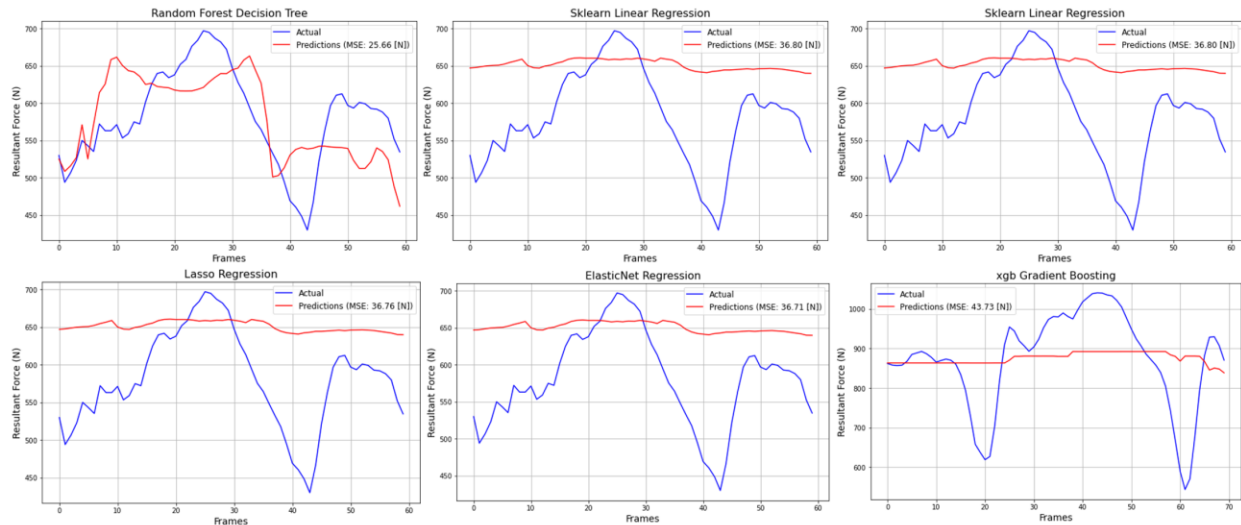


Figure 23 Actual vs Predicted Ground Reaction Forces using six different regression models for the first squat of the SLS.

A regression model which can most accurately capture the general expected shape of the resultant ground reaction forces of the second landing of the drop vertical jump and the trend imposed by the SLS is preferred. The general trend of the second landing of the DVJ starts off with a sudden peak in GRF due to the landing impact and then slowly tapers off to a near constant force reading. Figure 22 demonstrates that the random forest decision tree regression model is most adept at capturing the large peaks of the initial contact phase of the DVJ albeit a larger MSE than other models. Similar trends were observed for the SLS, shown in Figure 23, where the

random forest decision tree model could capture the peaks of the resultant GRF whereas other tested models stayed relatively flat in their force predictions and thus unable to capture an accurate trend. For these reasons, the random forest decision tree regression model was best suited for our application.

Distinct models were generated for each of the three exercises, tailored individually for both the right and left legs, utilizing exercise-specific training data. 51 DVJ's were used to train the DVJ regression models, 10 jumps were used to test the models. These jumps were cut to contain only the second landing to end of the jump phase. 75 SLS's were used to train the SLS regression models, 17 jumps were used to test the models. The entire recording was used for these jumps. 62 SLH's were used to train the SLH regression models and 19 were used in test. Unfortunately, we did not capture data of the subjects jumping onto the force plates for the SLH due to issues with potential injury and subject's discomfort with jumping onto the force plate with one leg. Therefore, only the portion of the recording from the start to toe-off was used to train the SLH models. Table 3 shows the mean squared error computed in Newtons (N) in the V, ML, and AP directions for all regression models tested on all available test jumps. It is important to note that there was no crossover between test subjects used in training and those featured in testing to avoid any model bias.

Table 3 Mean MSE (N) between actual GRF and predicted GRF for all test examples in all three force directions for DVJ, (Second Landing) SLS and SLH (start to toe-off phase)

Type	Side	ML (N)	AP (N)	V (N)
DVJ	Left Leg	33.21	41.64	220.20
	Right Leg	33.57	42.32	184.30
SLS	Left Leg	10.02	10.89	95.46
	Right Leg	12.87	12.02	156.58
SLH	Left Leg	45.27	14.38	127.90
	Right Leg	75.34	12.62	161.6

3.3.3 Exercise Metrics

Our KITS pose estimation software outputs many metrics for each performed exercise based on the time-series values. There are many standard metrics among all three exercises, and a few are specific to the SLH and SLS only since both exercises are performed on a specific leg. There are also some DVJ specific exercise metrics since we compute ratios between the first and second landing of the DVJ. Table 4 describes the metrics common to all exercises. All metrics are computed in degrees except for time to stabilization which is computed in seconds.

Table 4 Common Exercise Description

Metric Name	Description
Initial Coronal	Coronal knee angle at initial contact
Peak Valgus	Maximum valgus angle of the knee throughout the exercise
Peak Sagittal	Maximum moment of flexion throughout the exercise
Peak Coronal	Maximum coronal angle of the knee throughout the exercise
Max. Spine Sway	Maximum spine sway in X and Z directions throughout the exercise
Max. Pelvis Tilt	Maximum pelvis tilt angle in Y and Z directions throughout the exercise
Spine Sway Variability	Standard deviation of spine sway throughout the exercise in X and Z
Max. Neck Sway	Maximum neck sway angles in X and Z throughout the exercise
Max. Ankle Distance	Maximum ankle distance throughout the exercise
Max. Wrist Distance	Maximum wrist distance throughout the exercise
Mid Axis Sway Ratio	Ratio of number of frames which have positive spine sway angle over the number of total frames of exercise
Max. TBCM Sway	Maximum TBCM sway value subtracted by the minimum TBCM sway value [43]
TBCM Sway Deviation	Standard deviation of TBCM sway values throughout the exercise (refer to section 0 for more details)
Time to Stabilization (s)	*Refer to section 3.3.5

There are SLS and SLH specific metrics since both exercises are performed on one leg. The SLS and SLH are both performed on one leg; in order to distinguish between the two legs, the leg which the athlete jumps on will be referred to as the “supporting leg” (SL), and the other leg will be referred to as the “non-supporting leg” (NSL). Moreover, there are DVJ specific metrics containing ratio values between the first and second landing of the DVJ. These metrics are specific to the DVJ since it is the only exercise that contains two separate landing phases. These metrics were computed in order to compare standard deviation and maximum values between both landing

phases to attempt to discriminate between concussed and non-concussed individuals. Table 5 describes the metrics which are specific to each jump. All described metrics are measured in degrees except for the ratios which are unitless.

Table 5 Exercise-Specific Metrics Description

Exercise	Metric Name	Description
DVJ	Spine Sway Variability Landing Ratio	Ratio between spine sway standard deviation on first landing and second landing phases in both X and Z directions
	Max. Spine Sway Landing Ratio	Ratio between maximum spine sway value on first and second landing phases of jump in both X and Z directions
SLS & SLH	SL & NSL Coronal Variability	Standard deviation of coronal knee angle for both the SL and NSL
	SL & NSL Sagittal Variability	Standard deviation of sagittal knee angle for both the SL and NSL
	SL & NSL Max. Coronal	Maximum coronal knee angle of both the SL/NSL throughout the exercise
	SL & NSL Max. Sagittal	Maximum sagittal knee angle of both the SL and NSL throughout the exercise

3.3.4 TBCM Sway Implementation

Yeung et al. describe simple method for computing the total body centre of mass sway used for assessing balance control [43]. The summarized methodology of how TBCM sway is computed can be found in section 2.3 of this thesis. We were able to implement TBCM sway in our KITS software by first computing the TBCM point in the X-Y plane throughout time then by creating a vector between the TBCM point and the SpineBase point (only X and Y coordinates) on the body given by the Kinect V2. Subsequently, our software retrieves the maximum and minimum TBCM sway values for each recording and finally computes TBCM sway through the following simple equation [43]:

$$TBCM\ Sway = Max.TBCM\ Angle - Min.TBCM\ Angle \quad (11)$$

Figure 24 shows the implementation of the TBCM point in space and proves that the added point on the skeleton estimates well the true location of the centre of mass of the athlete.

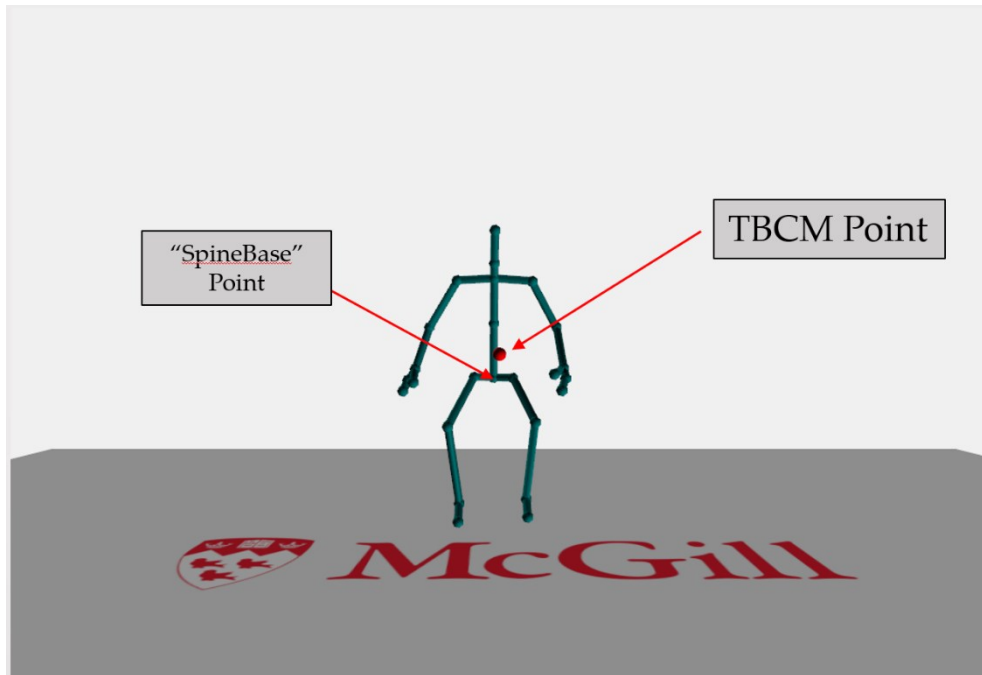


Figure 24 TBCM point (red) implementation in KITS software.

3.3.5 Time to Stabilization

Quoting Fransz et al., “Time to stabilization is the time it takes for an individual to return to baseline or stable state following a jump or hop landing” [59]. There are several varied methods for computing TTS. The study by Lynall et Al. computed TTS by fitting the resultant ground reaction force curve with a third order polynomial and defined TTS as the time it took for the fitted curve to fall below the GRF reference value. The GRF reference value was computed as the mean range of GRF variation plus three standard deviations (SD) [37]. There are many accepted methods for computing the GRF reference value [59]. The method that proved most fruitful in our study was the following:

$$Reference_{GRF} = TimeSeries Mean \pm 0.25 * SD \quad (12)$$

Due to the observed volatility of the GRF regression models at the beginning phases of each exercise, equation (12) was modified slightly to include the time-series median rather than the mean in order to be insensitive to outliers. Since the literature states that there is a range of values from [-0.25, 0.25] acceptable to adjust the GRF reference value by the standard deviation we define a parameter K which will be tuned to achieve most optimal results [59] :

$$Reference_{GRF} = TimeSeries Median \pm K * SD \quad (13)$$

Table 6 displays the p-values using a one-sided T-test when comparing TTS means for the recently concussed group and control group for various values for the K parameter. The concussion group is defined as those who have received one or more concussions within the last two years.

Table 6 TTS P-Value for different K values for all exercises

Exercise Type	K	TTS <i>p</i> -value
DVJ	-0.2	0.109
	-0.1	0.107
	-0.05	0.0456
	0.05	0.0459
SLS	-0.2	0.4745
	-0.1	0.4355
	-0.05	0.430
	0.05	0.4795
SLH	-0.2	0.2579
	-0.1	0.1995
	-0.05	0.177
	0.05	0.321

Table 6 demonstrates that a chosen hyperparameter $K = -0.05$ yields the most statistically significant results when comparing TTS between the concussed and control group for all exercise types. Figure 25 represents an example of the computation of TTS between using actual down sampled force plate data and forces obtained from the random forest decision tree regression model. It is important to note that if the subject never achieved stabilization, their TTS was calculated as the entire length of landing phase of the DVJ/SLH and the entire length of exercise for the SLS. Table 7 summarizes the percentage difference between the actual TTS and predicted TTS for the DVJ and SLS on the gathered test samples. Comparison results are not available for the SLH since we did not collect any force plate data of the subjects jumping onto the force plate.

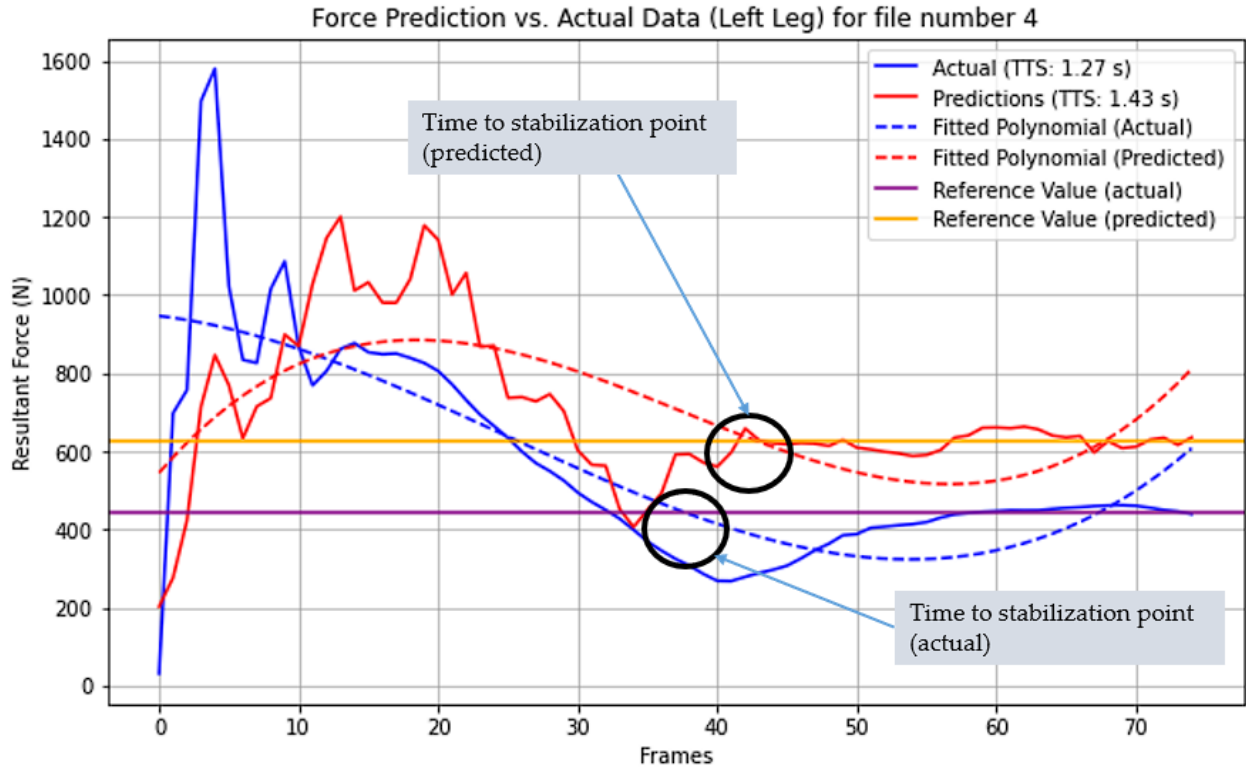


Figure 25 Example of Computation of Actual vs Predicted TTS for a DVJ

Table 7 Average and Median Percentage Change between Actual TTS (s) and Predicted TTS (s) for each model

Regression Model	Average (%)	Median (%)
DVJ Left Leg	24.73	17.08
DVJ Right Leg	31.37	22.18
SLS Left Leg	38.60	19.29
SLS Right Leg	20.28	17.93

Chapter 4 Results & Discussion

4.1 Leg Dominance Outcomes

The results for the SLS and SLH are separated between jumps performed on the athletes' dominant and non-dominant leg. Leg dominance for the SLH was determined by comparing the athletes forward jump distance on their left and right legs. Whichever leg the athlete jumped furthest on average is determined to be their dominant leg. For the SLS, leg dominance was defined as the leg in which the athlete had the highest average peak sagittal angle. Table 8 shows the leg dominance statistics for the 2022 and 2023 athletic cohorts given this strategy.

Table 8 Leg Dominance Statistics for 2022 and 2023 athletic cohorts

Year	Left Leg Dominant	Right Leg Dominant
2022	199	245
2023	176	255

It is important to note that this experiment does not consider whether athletes fall into a third category of footedness: mixed footers. According to a study by Tran and Voracek with 12,000 participants in 2016, 61.6% of the population is right-footed, 8.2% are left footed and 30.2% are mixed-footed [60]. When assessing leg dominance on the premise of jump distance or maximum peak flexion, the average values computed for each leg were close for many participants. It could be that for these people they fall into the mixed-legged category. However, for simplicity's sake we determined their footedness as a binary measure of either left or right based on which leg had higher jump distance or flexion angle, depending on the exercise. The percentage split of right-footed varsity athletes agrees with the study by Tran and Voracek and thus we were satisfied with the results [60].

4.2 DVJ, SLS, SLH Cross-Sectional Study Overall Outcomes

The regression models for the DVJ were used to predict TTS for the SLH. This was done due to lack of captured data of the subjects landing onto the force plate for SLH. It is presumed that the overall pattern of the landing phase in a DVJ is similar to that of the SLH, rendering DVJ models better suited for predicting GRF compared to SLH models. The latter, possessing lesser predictive power and solely comprising data from patients taking off from the force plate, are thus overshadowed by DVJ models.

The following tables demonstrate the results comparing metrics between those who sustained one or many concussions in the last two years compared to the control group. All metrics are reported in degrees except for TTS which is reported in seconds.

Table 9 Drop Vertical Jump Outcomes (statistically significant metrics shown by bolded rows)

Group

Metric	Control (n = 371)	Concussion (n = 84)	p-value
Initial Coronal Left	-1.961	-2.299	0.216
Initial Coronal Right	-2.026	-1.890	0.359
Peak Valgus Left	-2.833	-2.324	0.070
Peak Valgus Right	-2.871	-2.226	0.030
Peak Coronal Left	3.844	2.992	0.030
Peak Coronal Right	3.182	3.021	0.366
Peak Sagittal Left	93.940	88.646	0.021
Peak Sagittal Right	93.772	89.650	0.050
Max Spine Sway X	3.232	2.932	0.041
Max Spine Sway Z	41.219	37.611	0.014
Max Pelvis Tilt Y	4.098	3.411	< 0.001
Max Pelvis Tilt Z	1.532	1.292	0.005
Spine Sway X Variability	0.552	0.474	0.010
Spine Sway Z Variability	2.954	2.732	0.068
Spine Sway Variability Landing Ratio X	0.861	0.877	0.325
Spine Sway Variability Landing Ratio Z	1.083	1.143	0.153
Max. Spine Sway Landing Ratio X	1.153	1.038	0.093
Max. Spine Sway Landing Ratio Z	2.396	2.190	0.183
Mid Axis Sway	0.794	0.814	0.087
Max Neck Sway X	9.060	7.099	0.001
Max Neck Sway Z	21.682	21.533	0.441
Max Ankle Distance	0.336	0.319	0.022
Max Wrist Distance	0.580	0.577	0.410
Coronal Variability	0.596	0.543	0.154
Sagittal Variability	4.480	4.156	0.059
TBCM Sway	45.984	39.659	0.085
TBCM Sway Standard Deviation	12.136	10.0323	0.127
Time to Stabilization (s)	0.388	0.477	0.046

Table 10 Single Leg Squat Outcomes (statistically significant metrics shown by bolded rows)

Metric	Group		p-value
	Control (n = 353)	Concussion (n = 76)	
Dominant Leg			
Initial Coronal	6.507	6.480	0.470
Peak Valgus	1.773	1.361	0.251
Peak Coronal	10.174	9.792	0.272
Peak Sagittal	104.250	105.911	0.313
Max Spine Sway X	10.648	10.762	0.432
Max Spine Sway Z	42.826	44.210	0.234
Spine Sway Variability X	1.178	1.231	0.222
Spine Sway Variability Z	4.294	4.486	0.196
NSL Max Coronal	11.073	18.033	0.024
NSL Max Sagittal	97.245	97.852	0.460
Max Pelvis Tilt Y	12.980	12.838	0.429
Max Pelvis Tilt Z	3.835	4.304	0.150
Max Neck Sway X	19.472	18.855	0.339
Max Neck Sway Z	30.567	32.267	0.161
Max Wrist Distance	0.621	0.665	0.117
Max Ankle Distance	0.501	0.537	0.100
SL Coronal Variability	0.549	0.563	0.422
SL Sagittal Variability	4.044	4.300	0.150
NSL Coronal Variability	1.051	1.127	0.277
NSL Sagittal Variability	2.896	2.885	0.482
Time to Stabilization	1.173	1.212	0.340
Non-Dominant Leg			
Initial Coronal	5.827	6.011	0.269
Peak Valgus	2.083	2.052	0.482
Peak Coronal	8.820	8.641	0.372
Peak Sagittal	88.464	86.325	0.218
Max Spine Sway X	9.247	9.112	0.389
Max Spine Sway Z	38.784	38.306	0.394
Spine Sway Variability X	1.150	1.020	0.067
Spine Sway Variability Z	4.174	3.912	0.180
NSL Max Coronal	11.849	12.969	0.354
NSL Max Sagittal	83.079	84.201	0.422
Max Pelvis Tilt Y	11.096	10.455	0.159
Max Pelvis Tilt Z	3.782	2.917	0.028
Max Neck Sway X	16.320	14.822	0.095
Max Neck Sway Z	27.721	28.865	0.227
Max Wrist Distance	0.708	0.578	0.129
Max Ankle Distance	0.676	0.453	0.090

SL Coronal Variability	0.466	0.416	0.077
SL Sagittal Variability	3.339	3.474	0.195
NSL Coronal Variability	0.924	0.940	0.450
NSL Sagittal Variability	2.472	2.434	0.427
Time to Stabilization (s)	1.072	1.046	0.346

Table 11 Single Leg Hop Outcomes (statistically significant metrics shown by bolded rows)

Metric	Group		p-value
	Control (n = 395)	Concussion (n = 38)	
Dominant Leg			
Initial Coronal	2.989	3.162	0.370
Peak Valgus	-1.134	-0.611	0.190
Peak Coronal	7.970	8.363	0.319
Peak Sagittal	76.840	74.888	0.293
Max Spine Sway X	11.389	11.772	0.279
Max Spine Sway Z	34.300	32.871	0.238
Spine Sway Variability X	0.418	0.478	0.093
Spine Sway Variability Z	0.704	0.722	0.405
NSL Max Coronal	2.103	-2.926	0.032
NSL Max Sagittal	100.418	98.216	0.274
Max Pelvis Tilt Y	13.287	14.110	0.202
Max Pelvis Tilt Z	2.805	2.603	0.151
Max Neck Sway X	20.627	21.146	0.375
Max Neck Sway Z	29.247	31.683	0.102
Max Wrist Distance	0.764	0.747	0.322
Max Ankle Distance	0.549	0.532	0.207
SL Coronal Variability	0.727	0.776	0.341
SL Sagittal Variability	2.801	2.851	0.420
NSL Coronal Variability	1.193	1.272	0.336
NSL Sagittal Variability	2.579	2.495	0.379
Time to Stabilization (s)	0.944	0.849	0.026
Non-Dominant Leg			
Initial Coronal	3.143	3.051	0.393
Peak Valgus	-0.189	-0.243	0.461
Peak Coronal	6.683	6.336	0.302
Peak Sagittal	64.156	65.114	0.369
Max Spine Sway X	10.046	10.415	0.328
Max Spine Sway Z	28.885	29.139	0.449
Spine Sway Variability X	0.350	0.378	0.153
Spine Sway Variability Z	0.590	0.642	0.239
NSL Max Coronal	0.569	2.904	0.104

NSL Max Sagittal	84.836	87.219	0.166
Max Pelvis Tilt Y	11.555	12.264	0.257
Max Pelvis Tilt Z	2.470	2.614	0.264
Max Neck Sway X	17.796	18.703	0.320
Max Neck Sway Z	25.150	28.008	0.041
Max Wrist Distance	0.644	0.687	0.057
Max Ankle Distance	0.464	0.437	0.090
SL Coronal Variability	0.530	0.464	0.079
SL Sagittal Variability	2.180	2.111	0.339
NSL Coronal Variability	0.980	0.881	0.104
NSL Sagittal Variability	2.099	2.045	0.358
Time to Stabilization (s)	0.803	0.825	0.301

The results presented in Table 9 demonstrate twelve statistically significant differences in exercise metrics for the DVJ which was the most out of all three exercises. The concussion group had lower peak valgus right, peak coronal left, peak sagittal left & right max spine sway X & Z, max pelvis tilt Y & Z, max neck sway X and max ankle distance. These trends could indicate that the concussed group exhibit stiffer jumping mechanics due to their history of concussion compared to the control group. These findings are in line with studies that show higher neck, knee, ankle, hip stiffness in concussed athletes compared to healthy athletes [4], [5], [34]. Of particular importance are the TTS differences between concussed (mean = 0.477 seconds) and control (mean = 0.388 seconds) groups ($p = 0.046$). This statistic indicates that those with concussion history take longer to stabilize on the landing phase of the DVJ compared to the healthy controls.

The results presented in Table 10 indicate only two statistically significant differences in exercise metrics for the SLS between concussed and control groups. When jumping on their dominant leg, the concussed group has a higher mean non-supporting maximum coronal knee angle than the control group. A higher maximum coronal angle on the non-supporting leg may indicate difficulties in achieving stable balance during the SLS movement. The overall results of the SLS indicate no significant group differences which is consistent with the findings found by Lynall et al [37].

The results presented in Table 11 indicate only three statistically significant differences between concussed and control groups. For the dominant leg, the concussed group had a significantly lower and opposite-signed non-supporting maximum coronal knee angle which indicates the concussed group favor the opposite direction on their non-supporting leg when attempting balance on the SLH. Maximum neck sway in the Z direction is higher for jumps on the non-dominant leg for the concussed group which indicates a more dramatic neck ‘bobble’ which is a long-term persistent concussion symptom [4], [5]. Time to stabilization on the dominant leg is significantly lower for the concussed group than the control group which is counter to the expected trend. This could be because concussed candidates at McGill university go through extensive balance rehabilitation after concussion and are therefore more adept at achieving stability on a SLH compared to those who have gone through minimal balance rehabilitation. No group differences in TTS were observed for the non-dominant leg.

4.3 DVJ, SLS and SLH Cross-Sectional Gender-Based Outcomes

The physiological differences between males and females results in varied performance for the mentioned aerobic exercises and thus accentuates the need for a gender-based analysis of the athlete’s movement mechanics and balance capabilities to understand which exercise and which metrics best discriminate between concussed and healthy controls for males and females. Table 12,

Table 13 and

Table 14 demonstrates the outcomes separately for males and females for the DVJ, SLS and SLH, respectively.

Table 12 Comparison of Metrics Between Control and Concussion Groups by Gender for DVJ (Statistically Significant Metrics shown by Bolded Rows)

Metric	Group = Male		p-value	Group = Female		p-value
	Control (n = 231)	Concussion (n = 53)		Control (n = 140)	Concussion (n = 31)	
Initial Coronal Left	-1.373	-1.624	0.329	-2.931	-3.454	0.194
Initial Coronal Right	-1.623	-1.495	0.401	-2.691	-2.566	0.404
Peak Valgus Left	-2.229	-1.627	0.075	-3.829	-3.514	0.280
Peak Valgus Right	-2.355	-1.876	0.149	-3.721	-2.824	0.032
Peak Coronal Left	4.863	3.699	0.017	2.163	1.783	0.305
Peak Coronal Right	4.079	3.588	0.221	1.703	2.050	0.294
Peak Sagittal Left	95.042	89.025	0.041	92.121	87.998	0.147
Peak Sagittal Right	94.850	89.577	0.061	92.007	89.532	0.262
Max Spine Sway X	3.231	2.711	0.009	3.234	3.311	0.391
Max Spine Sway Z	43.118	37.455	0.005	38.086	37.880	0.466
Max Pelvis Tilt Y	4.101	3.165	< 0.001	4.094	3.831	0.212
Max Pelvis Tilt Z	1.487	1.162	0.003	1.605	1.516	0.272
Spine Sway X Variability	0.564	0.477	0.021	0.532	0.469	0.124
Spine Sway Z Variability	3.177	2.903	0.094	2.588	2.441	0.207
Max Neck Sway X	9.177	6.614	< 0.001	8.866	7.928	0.183
Max Neck Sway Z	23.783	22.472	0.143	18.214	19.929	0.155
Max Ankle Distance	0.343	0.319	0.023	0.325	0.318	0.282
Max Wrist Distance	0.605	0.613	0.337	0.540	0.515	0.096
Coronal Variability	0.639	0.524	0.034	0.525	0.577	0.286
Sagittal Variability	4.428	3.955	0.033	4.565	4.500	0.426
Time to Stabilization (s)	0.437	0.476	0.270	0.374	0.586	0.070

Table 13 Comparison of Metrics Between Control and Concussion Groups by Gender for SLS (Statistically Significant Metrics shown by Bolded Rows)

Metric	Group = Male		p-value	Group = Female		p-value
	Control (n = 231)	Concussion (n = 45)		Control (n = 142)	Concussion (n = 31)	
Dominant Leg						

Initial Coronal	6.838	6.704	0.394	6.015	6.155	0.388
Peak Valgus	1.997	0.873	0.103	1.440	2.069	0.213
Peak Coronal	10.688	9.733	0.131	9.411	9.878	0.309
Peak Sagittal	106.018	110.062	0.201	101.622	99.886	0.348
Max Spine Sway X	11.095	10.622	0.249	9.984	10.965	0.226
Max Spine Sway Z	43.571	43.690	0.480	41.720	44.964	0.156
Spine Sway Variability X	1.200	1.298	0.166	1.146	1.135	0.447
Spine Sway Variability Z	4.338	4.472	0.332	4.228	4.507	0.200
NSL Max Coronal	9.868	20.344	0.008	12.864	14.679	0.381
NSL Max Sagittal	96.479	100.481	0.303	98.384	94.034	0.326
Max Pelvis Tilt Y	13.250	12.900	0.357	12.578	12.748	0.452
Max Pelvis Tilt Z	3.742	4.411	0.141	3.973	4.148	0.395
Max Neck Sway X	20.146	20.726	0.387	18.471	16.140	0.138
Max Neck Sway Z	32.343	34.550	0.152	27.929	28.952	0.355
Max Wrist Distance	0.668	0.683	0.369	0.551	0.638	0.082
Max Ankle Distance	0.517	0.533	0.310	0.477	0.542	0.103
SL Coronal Variability	0.537	0.582	0.316	0.569	0.535	0.357
SL Sagittal Variability	4.116	4.567	0.122	3.936	3.911	0.455
NSL Coronal Variability	1.029	1.235	0.139	1.083	0.972	0.247
NSL Sagittal Variability	2.919	3.107	0.295	2.861	2.561	0.147
Time to Stabilization (s)	1.204	1.283	0.274	1.128	1.108	0.437
Non-Dominant Leg						
Initial Coronal	6.002	6.034	0.469	5.568	5.975	0.178
Peak Valgus	2.082	1.588	0.286	2.083	2.772	0.252
Peak Coronal	8.762	8.141	0.205	8.907	9.417	0.251
Peak Sagittal	88.428	89.596	0.374	88.516	81.249	0.036
Max Spine Sway X	9.585	9.514	0.458	8.750	8.490	0.343
Max Spine Sway Z	39.270	39.366	0.484	38.066	36.660	0.288
Spine Sway Variability X	1.114	1.093	0.395	1.202	0.907	0.048
Spine Sway Variability Z	4.135	4.073	0.432	4.233	3.662	0.107
NSL Max Coronal	11.784	13.323	0.344	11.945	12.420	0.462
NSL Max Sagittal	82.004	89.110	0.191	84.664	76.583	0.137
Max Pelvis Tilt Y	11.486	11.043	0.311	10.519	9.543	0.123
Max Pelvis Tilt Z	3.770	2.927	0.096	3.799	2.902	0.064
Max Neck Sway X	17.189	16.703	0.380	15.038	11.904	0.014
Max Neck Sway Z	28.846	31.620	0.071	26.060	24.590	0.272
Max Wrist Distance	0.696	0.612	0.252	0.724	0.525	0.177
Max Ankle Distance	0.649	0.467	0.188	0.714	0.431	0.155
SL Coronal Variability	0.446	0.421	0.278	0.497	0.409	0.081
SL Sagittal Variability	3.352	3.711	0.059	3.320	3.106	0.114
NSL Coronal Variability	0.902	1.039	0.240	0.957	0.787	0.089
NSL Sagittal Variability	2.481	2.641	0.295	2.459	2.113	0.094
Time to Stabilization (s)	1.107	1.114	0.470	1.020	0.940	0.217

Table 14 Comparison of Metrics Between Control and Concussion Groups by Gender for SLH
(Statistically Significant Metrics shown by Bolded Rows)

Metric	Group		p-value	Group		p-value
	Control (n = 249)	Concussion (n = 26)		Control (n = 146)	Concussion (n = 12)	
Dominant Leg						
Initial Coronal	3.471	2.884	0.206	2.166	3.763	0.006
Peak Valgus	-1.011	-1.151	0.429	-1.343	0.559	0.013
Peak Coronal	8.364	7.903	0.340	7.300	9.360	0.039
Peak Sagittal	79.781	76.640	0.263	71.825	71.090	0.427
Max Spine Sway X	11.612	11.648	0.482	11.008	12.039	0.206
Max Spine Sway Z	36.506	34.935	0.273	30.539	28.398	0.208
Spine Sway Variability X	0.413	0.458	0.189	0.425	0.521	0.162
Spine Sway Variability Z	0.725	0.801	0.226	0.669	0.553	0.070
NSL Max Coronal	3.790	1.882	0.257	-0.775	-13.343	0.006
NSL Max Sagittal	101.166	97.565	0.209	99.143	99.624	0.472
Max Pelvis Tilt Y	13.646	14.716	0.210	12.674	12.796	0.461
Max Pelvis Tilt Z	2.790	2.744	0.428	2.829	2.298	0.033
Max Neck Sway X	21.539	21.744	0.460	19.073	19.851	0.387
Max Neck Sway Z	32.344	34.329	0.177	23.966	25.951	0.283
Max Wrist Distance	0.801	0.743	0.076	0.701	0.756	0.250
Max Ankle Distance	0.578	0.551	0.126	0.501	0.491	0.409
SL Coronal Variability	0.751	0.846	0.281	0.687	0.626	0.335
SL Sagittal Variability	2.912	2.934	0.472	2.612	2.670	0.444
NSL Coronal Variability	1.129	1.183	0.388	1.302	1.465	0.356
NSL Sagittal Variability	2.542	2.672	0.359	2.642	2.112	0.085
Time to Stabilization	0.934	0.818	0.031	0.961	0.914	0.279
Non-Dominant Leg						
Initial Coronal	3.455	3.057	0.188	2.605	3.040	0.175
Peak Valgus	0.038	-0.686	0.150	-0.580	0.717	0.085
Peak Coronal	6.759	6.691	0.465	6.554	5.566	0.236
Peak Sagittal	65.231	68.615	0.166	62.305	57.527	0.153
Max Spine Sway X	9.871	10.616	0.245	10.348	9.979	0.387
Max Spine Sway Z	30.053	31.361	0.305	26.874	24.324	0.172
Spine Sway Variability X	0.333	0.393	0.040	0.381	0.343	0.162
Spine Sway Variability Z	0.594	0.732	0.077	0.586	0.447	0.037
NSL Max Coronal	0.906	0.927	0.412	-2.323	-0.678	0.314
NSL Max Sagittal	2.030	2.194	0.176	86.365	82.812	0.217
Max Pelvis Tilt Y	11.413	12.324	0.262	11.800	12.134	0.419
Max Pelvis Tilt Z	2.393	2.638	0.205	2.603	2.563	0.454
Max Neck Sway X	17.896	19.310	0.293	17.623	17.389	0.465
Max Neck Sway Z	27.224	30.054	0.057	21.576	23.575	0.268
Max Wrist Distance	0.664	0.702	0.126	0.610	0.655	0.178
Max Ankle Distance	0.478	0.467	0.332	0.440	0.371	0.006

SL Coronal Variability	0.516	0.526	0.432	0.554	0.330	0.001
SL Sagittal Variability	2.200	2.298	0.322	2.146	1.706	0.044
NSL Coronal Variability	0.906	0.927	0.412	1.108	0.782	0.011
NSL Sagittal Variability	2.030	2.194	0.176	2.218	1.722	0.037
Time to Stabilization (s)	0.778	0.854	0.075	0.845	0.762	0.152

The results demonstrated by Table 12 show that, when performing the DVJ, there are eleven metrics that significantly discriminate between concussed and healthy controls for males whereas only one metric discriminates between groups for females when performing the DVJ. All significant metrics are lower for the concussed group compared to the control which signifies stiffer overall movement for the injured cohort. For the SLS,

Table 13 returns a single metric for males and two for females which are significantly different between concussed and healthy controls. Concussed females have lower neck sway in the X direction compared to healthy controls which may be a sign of neck pain, a long-term persistent concussion symptom [4], [5]. Furthermore, injured female athletes have a significantly lower peak sagittal angle on their non-dominant leg compared to healthy controls, indicating that injured female athletes squat less extremely on their non-dominant leg. Concussed males have a significantly higher maximum coronal angle on the NSL which may indicate difficulties at achieving stable balance as their NSL is swaying more drastically during the SLS movement than the healthy controls.

Table 14 demonstrates only two statistically significant metrics for males when performing the SLH whereas females display higher discriminatory power returning eleven statistically significant metrics between injured and healthy controls. Of important note is the significantly lower time to stabilization on the dominant leg for males which is counter to the expected trend and similarly demonstrated by the overall analysis results.

4.4 DVJ Prospective Analysis Outcomes

The previous studies were conducted in a cross-sectional view where the metrics of different people (concussed vs. not concussed) were being compared. A prospective study which compares exercise metrics of the same athletes who sustained one or many concussions from 2022 to 2023 is of utmost importance. The DVJ was the only exercise performed in both 2022 and 2023. This study will determine whether an athlete's movement mechanics during a DVJ change if they have sustained one of many concussions within the past year. We will compare only athletes who performed three DVJs in 2022 and 2023 and compare their average metrics in both years to ascertain any significant statistical differences. Figure 26 explains the data flow chart of the athletes which jumped in both 2022 and 2023.

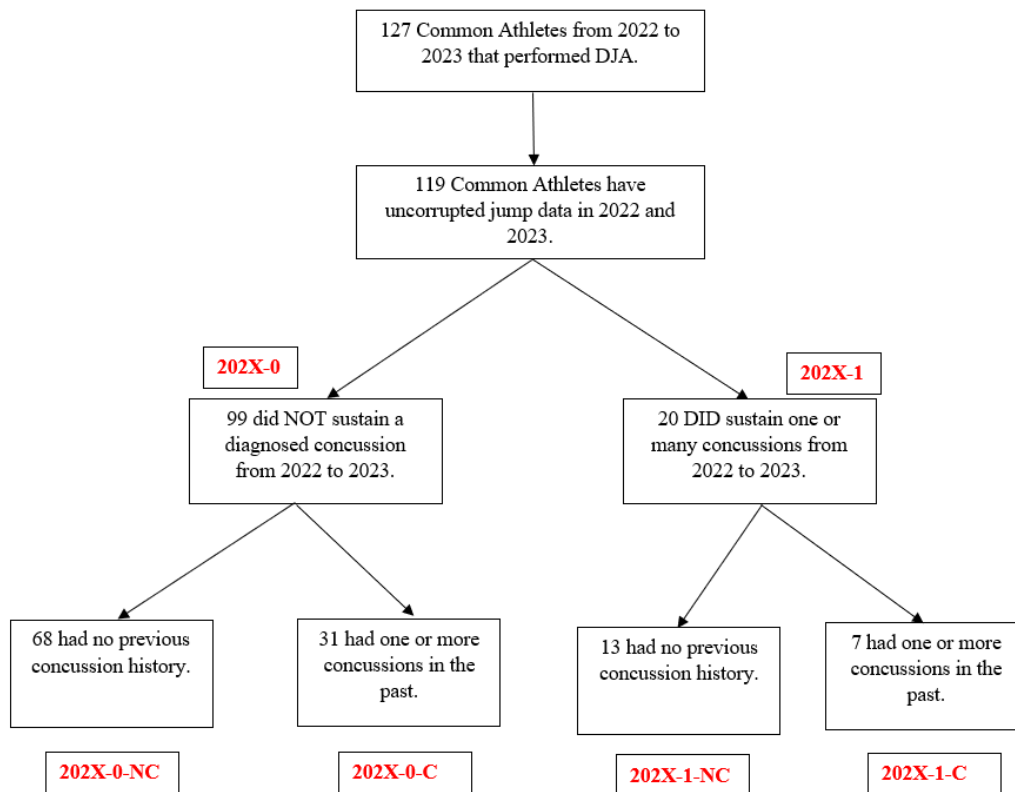


Figure 26 Prospective Study Data Flow Chart Breakdown

Each block in the data flow chart is indicated by a red code used for quickly identifying the group. 202X refers to the year the athletes performed the exercises where $X = \{2,3\}$. Those who fall into the “-0” group did not sustain a diagnosed concussion from 2022 to 2023 whereas those who fall into the “-1” group sustained one or many concussions from 2022 to 2023. Both of these groups can be split into two additional groups of those who had previous concussion history and those who had none. Those who had no previous concussion history fall into the “-NC” group whereas those who had previous concussion history fall under the “-C” group. For example, 2022-0-NC refers to the group who had no previous concussion history, did not sustain a concussion in the last year and are examining their exercise statistics in 2022. Figure 26 shows that of the 119 athletes which jumped in both 2022 and 2023 that had uncorrupted data, only 20 of them sustained a concussion from 2022 to 2023. This group of 20 will be our examined cohort in our prospective study. It is important to note that these individuals only performed exercises during their pre-season physicals in each respective year. No other data collection occurred throughout the rest of their varsity seasons. Table 15 compares the DVJ exercise metrics of the 20 athletes which sustained one or many concussions before and after their injury.

Table 15 Prospective Study Mean Outcomes (DVJ), all metrics computed in degrees except for ratios which are unitless and time to stabilization which is in seconds.

Metric	Jump Year		p-value
	2022 (n = 20)	2023 (n = 20)	
Initial Coronal Left	-1.697	-0.845	0.228
Initial Coronal Right	-2.498	-1.424	0.116
Peak Valgus Left	-3.545	-2.325	0.128
Peak Valgus Right	-2.980	-2.648	0.346
Peak Coronal Left	5.530	3.880	0.082
Peak Coronal Right	4.057	3.314	0.266
Peak Sagittal Left	105.656	91.743	0.011
Peak Sagittal Right	105.007	91.300	0.013
Max Spine Sway X	4.367	3.405	0.048
Max Spine Sway Z	45.988	41.597	0.162
Max Pelvis Tilt Y	4.762	3.915	0.062
Max Pelvis Tilt Z	1.830	1.444	0.070
Spine Sway X Variability	1.019	0.799	0.066
Spine Sway Z Variability	5.566	6.248	0.263
Spine Sway Variability Landing Ratio X	0.743	0.702	0.316
Spine Sway Variability Landing Ratio Z	0.913	1.029	0.214
Max. Spine Sway Landing Ratio X	1.262	1.009	0.173
Max. Spine Sway Landing Ratio Z	2.568	2.040	0.215
Mid Axis Sway Ratio	0.827	0.772	0.151
Max Neck Sway X	13.597	13.679	0.489
Max Neck Sway Z	27.947	27.495	0.441
Max Ankle Distance	0.380	0.363	0.248
Max Wrist Distance	0.594	0.573	0.344
Coronal Variability	0.747	0.748	0.498
Sagittal Variability	5.494	5.310	0.367
TBCM Sway	57.980	45.668	0.169
TBCM Sway Standard Deviation	16.301	13.295	0.280
Time to Stabilization (s)	0.270	0.264	0.465

The results of the prospective study illustrate that there are no significant differences in exercise mechanics of those who sustained one or many concussions from 2022 to 2023 other than significantly lower peak sagittal left, right and maximum spine sway X angles post-injury. Lower sagittal angles suggests that athletes are not squatting as far down while performing the DVJ post-injury. This may be due to dynamic balance deficits exhibited in the injured athletes and hence their reluctance to squat to their fullest potential during a DVJ after recovering from mTBI. A decrease in maximum spine sway in the X-direction suggests that the athlete's movement is stiffer post-injury since they are swaying less extremely. An interesting result is the decrease in initial coronal, peak valgus, peak coronal, maximum spine sway, maximum pelvis tilt, maximum ankle distance, maximum wrist distance and TBCM Sway after concussion. Although none of the

mentioned metrics present a p -value < 0.05 , the slight decrease in metrics suggests the athletes mechanics are slightly stiffer and more reserved after concussion. Of note was the time to stabilization differences before concussion (mean = 0.270 seconds) and after concussion (mean = 0.264 seconds) which showed very little discriminatory power ($p = 0.465$).

Splitting the recently concussed group and control groups into those who had previous concussion history and those who had none (as shown in Figure 26), presents a very similar story. The exercise mechanics of the groups remain the same from 2022 to 2023 except for only two metrics which present interesting, yet opposite, stories. Figure 27 displays the mean max spine sway landing ratio in the X direction for all examined groups.

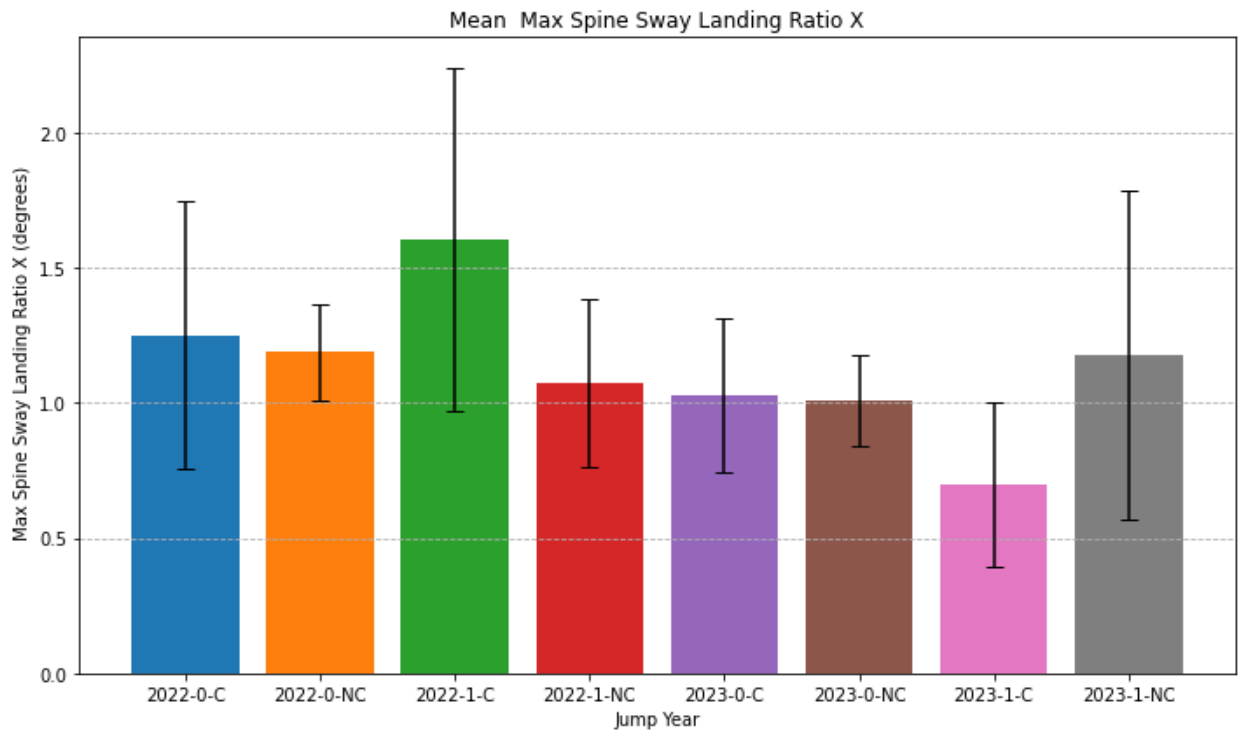


Figure 27 Mean Max Spine Sway Landing Ratio X compared across years (2022 and 2023) for those who did not sustain a concussion from year to year and those who did (-0, -1) and those who had no previous concussion history and those who did (-NC, -C).

The group that did not sustain a concussion year-to-year, represented by the blue, orange, purple, and brown bars, did not exhibit any significant changes in their jumping performance over time, regardless of their previous concussion history. In contrast, the group that did sustain a concussion year-to-year, represented by the green, red, pink, and grey bars, showed variations in their jumping performance over time if they had a previous concussion history. However, those within this concussed group who had no prior concussion history did not show differences in their jumping performance year-to-year.

The only other metric which showed an interesting discrepancy was the mean maximum neck sway in the X direction. Figure 28 shows the results.

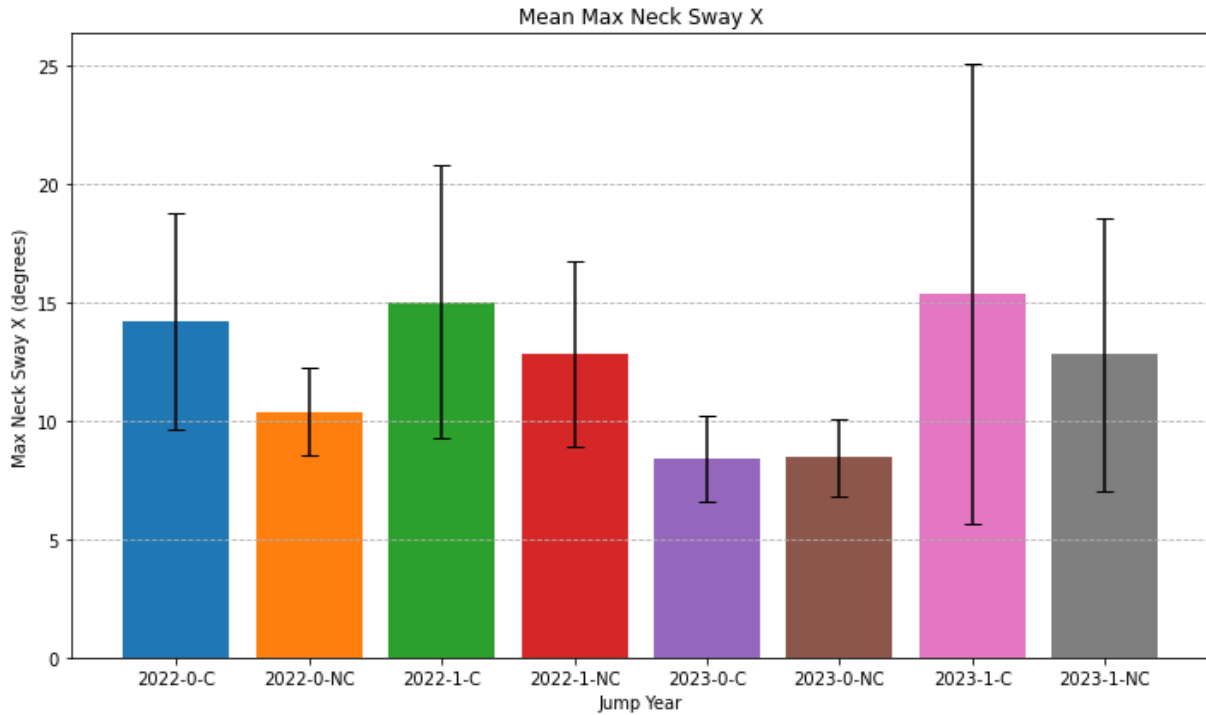


Figure 28 Mean Maximum Neck Sway X compared across years (2022 and 2023) for those who did not sustain a concussion from year to year and those who did (-0, -1) and those who had no previous concussion history and those who did (-NC, -C).

The group that did not sustain a concussion year-to-year, represented by the blue, orange, purple, and brown bars, exhibited different jumping patterns if they had a previous concussion history, while those without a previous concussion history did not show any changes in their jumping performance. On the other hand, the group that did sustain a concussion year-to-year, represented by the green, red, pink, and grey bars, did not demonstrate any differences in their jumping performance over time, regardless of whether they had a previous concussion history or not. All other metrics returned no significantly discriminatory results and further proves that despite sustaining one or many concussions in the last year, athletes are performing the DVJ similarly before and after injury even when accounting for whether the athlete had previous concussion history or not. The results of the prospective study suggest that despite recent mTBI injury or presence of concussion history or lack thereof, athletes are still jumping relatively the same way from one year to the next except for a few noteworthy results.

The intra-jump variability (IJV) of each participant was studied to ascertain any notable differences between their jumps in 2022 and 2023. IJV was computed by simply taking the standard deviation of the metrics across a single participant's jumps. A person with low IJV means they are jumping similarly for each trial whereas a person with high IJV corresponds to an individual who jumps differently each time. Table 16 shows the IJV results comparing jumps in 2022 to 2023 for the 20 athletes who sustained one or many concussions in the past year.

Table 16 Prospective Study IJV Outcomes (DVJ), all metrics computed in degrees except for ratios which are unitless and time to stabilization which is in seconds.

Metric	Jump Year		p-value
	2022 (n = 20)	2023 (n = 20)	
Initial Coronal Left	1.501	2.150	0.157
Initial Coronal Right	1.145	1.753	0.120
Peak Valgus Coronal Left	1.144	1.805	0.116
Peak Valgus Right	0.980	1.443	0.128
Absolute Peak Coronal Left	2.315	2.491	0.429
Peak Coronal Right	1.523	1.957	0.143
Peak Sagittal Left	5.808	15.708	0.007
Peak Sagittal Right	4.632	15.285	0.006
Max Spine Sway X	1.230	0.988	0.175
Max Spine Sway Z	4.027	6.120	0.081
Max Pelvis Tilt Y	1.216	1.359	0.276
Max Pelvis Tilt Z	0.534	0.485	0.365
Spine Sway X Variability	0.227	0.161	0.073
Spine Sway Z Variability	0.415	0.724	0.024
Spine Sway Variability Landing Ratio X	0.160	0.223	0.092
Spine Sway Variability Landing Ratio Z	0.154	0.237	0.075
Max. Spine Sway Landing Ratio X	0.604	0.601	0.495
Max. Spine Sway Landing Ratio Z	0.830	0.957	0.395
Mid Axis Sway Ratio	0.094	0.110	0.207
Max Neck Sway X	4.862	3.552	0.135
Max Neck Sway Z	3.338	3.950	0.200
Max Ankle Distance	0.017	0.029	0.022
Max Wrist Distance	0.050	0.044	0.395
Coronal Variability	0.201	0.197	0.476
Sagittal Variability	0.770	1.104	0.075
TBCM Sway	20.102	18.210	0.413
TBCM Sway Standard Deviation	7.657	7.059	0.431
Time to Stabilization (s)	0.147	0.128	0.346

The results of the study demonstrate that intra jump variability does not change after injury for any of the metrics other than peak sagittal left, peak sagittal right, spine sway variability in the Z direction and maximum ankle distance, all of which present higher IJV values post-injury. The 20 participants' spine sway variability metric in the x-direction varied more jump-to-jump after injury than before. This could be a sign of balance difficulties post-injury leading to higher inconsistency in their jump-to-jump mechanics related to their spine sway. Furthermore, the participants sagittal angle varies significantly more from one jump to the next post-injury compared to before sustaining an mTBI. This could suggest potential disruptions in neuromuscular control or balance, indicating that the mTBI has had a lasting impact on their motor coordination

and stability. Although all other metrics had less discriminatory power, 16 metrics presented higher intra-jump variability post-injury whereas 11 metrics had lower intra-jump variability post-injury.

Splitting the recently concussed group and control groups into those who had previous concussion history and those who had none (as shown in Figure 26), the story remains relatively the same. The IJV of the groups remain the same from 2022 to 2023 except for only three metrics which present notable results. Figure 29 displays the IJV for the spine sway variability metric in the X-direction.

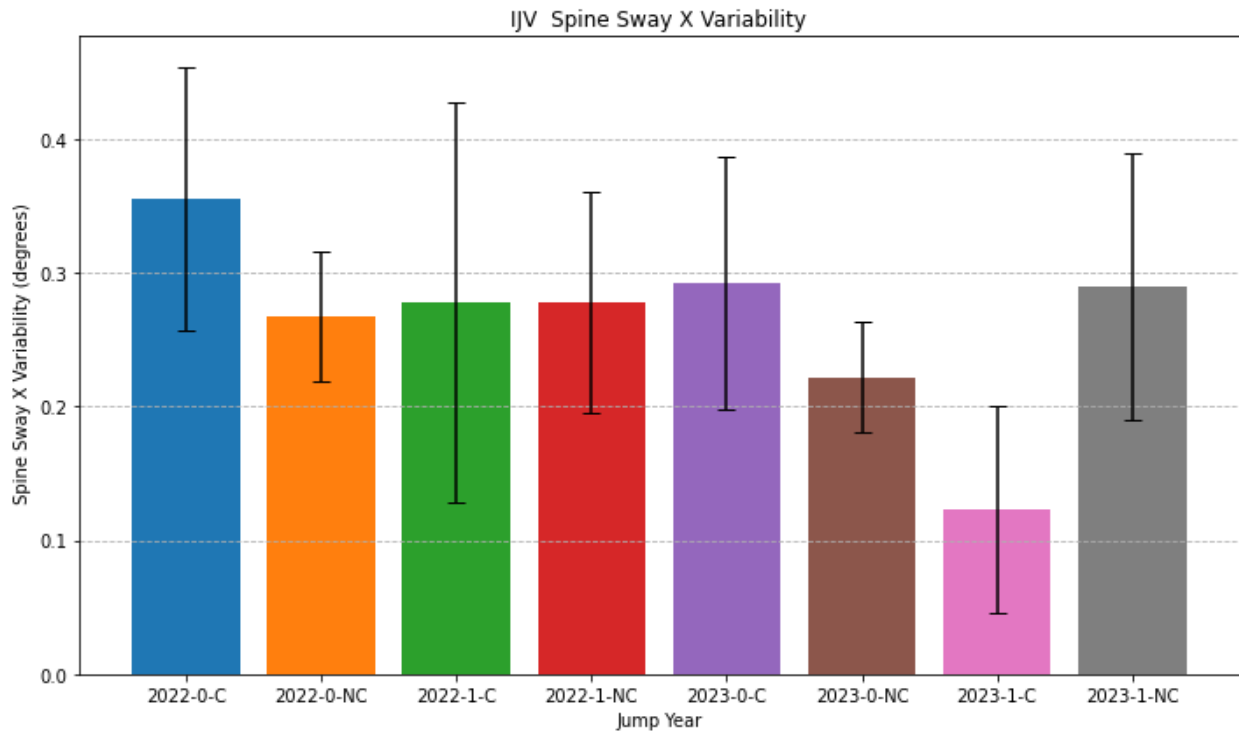


Figure 29 IJV Spine Sway X Variability compared across years (2022 and 2023) for those who did not sustain a concussion from year to year and those who did (-0, -1) and those who had no previous concussion history and those who did (-NC, -C).

The group that did not sustain a concussion year-to-year, represented by the blue, orange, purple, and brown bars, did not exhibit any differences in their jumping performance over time, regardless of their previous concussion history. In contrast, the group that did sustain a concussion year-to-year, represented by the green, red, pink, and grey bars, showed similar jumping performance in 2022 between those with and without previous concussion history. However, after recovering from a concussion in 2023, those with a previous concussion history had significantly lower IJV spine sway variability in the X direction compared to those with no previous concussions. This indicates that those with previous concussion history actually had improved IJV values for spine sway variability after recovering from injury. The maximum spine sway landing ratio also presents interesting results when examined from this viewpoint, shown in Figure 30.

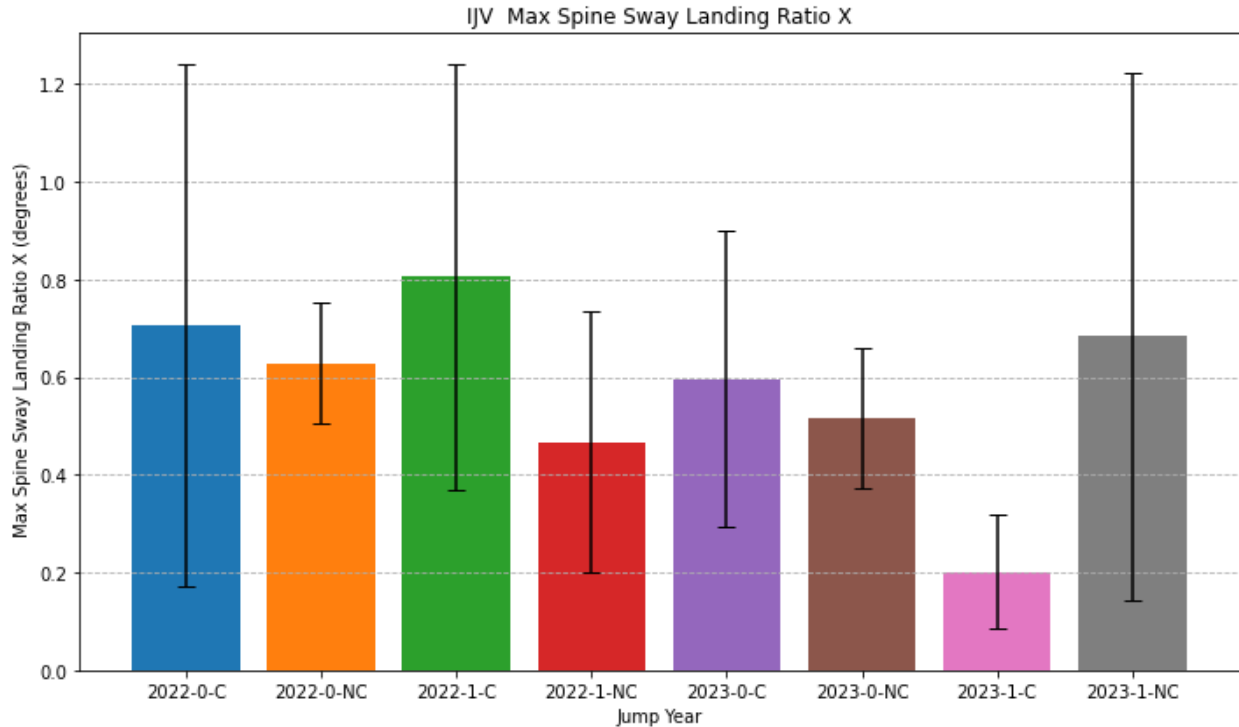


Figure 30 IJV Maximum spine sway landing ratio X compared across years (2022 and 2023) for those who did not sustain a concussion from year to year and those who did (-0, -1) and those who had no previous concussion history and those who did (-NC, -C).

The group that did not sustain a concussion year-to-year, represented by the blue, orange, purple, and brown bars, did not show any differences in their jumping performance regardless of their previous concussion history. In contrast, the group that did sustain a concussion year-to-year, represented by the green, red, pink, and grey bars, exhibited the same jumping performance in 2022. However, in 2023, those with a previous concussion history had a significantly lower Max Spine Sway Landing Ratio X IJV compared to their performance in 2022, while those without a previous concussion history showed similar IJV for this metric in 2023 as they did in 2022. These findings presents present a similar trend found with spine sway variability, where the group with concussion history had improved IJV results post-injury. Finally, the only other metric that returned a notable result is the maximum ankle distance shown in Figure 31

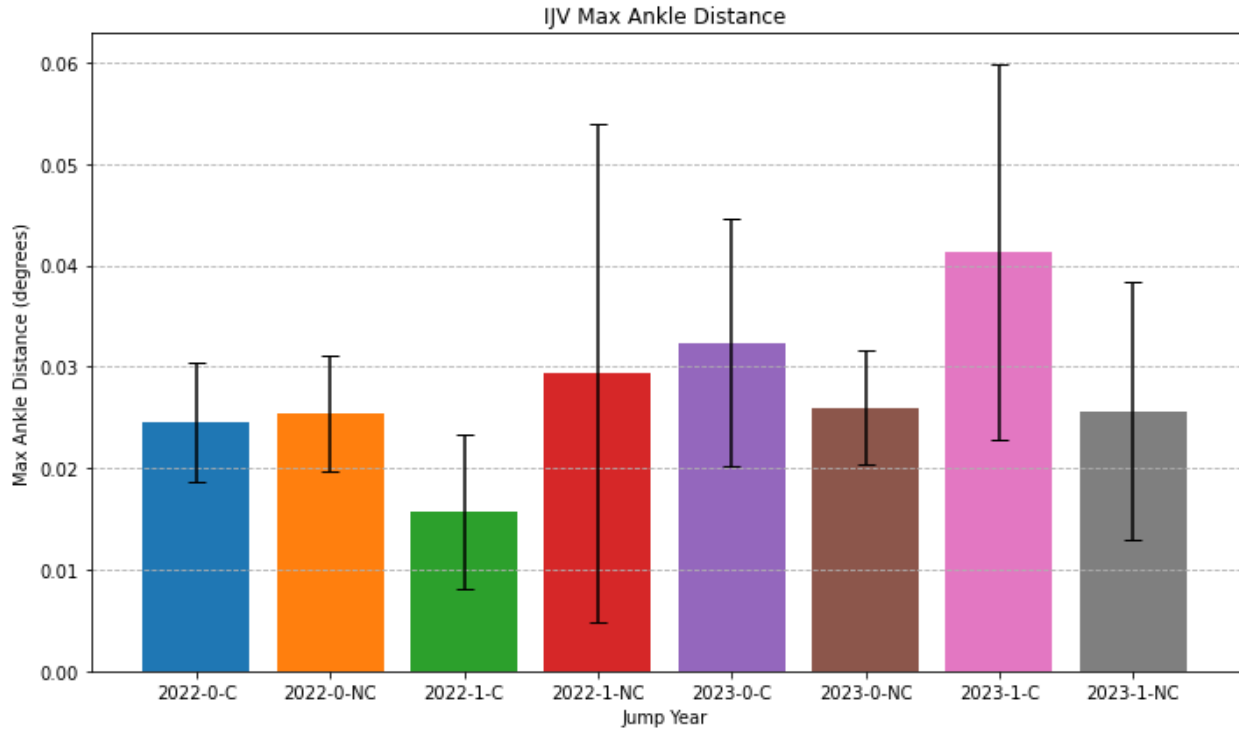


Figure 31 IJV Maximum ankle distance compared across years (2022 and 2023) for those who did not sustain a concussion from year to year and those who did (-0, -1) and those who had no previous concussion history and those who did (-NC, -C).

The group that did not sustain a concussion year-to-year, represented by the blue, orange, purple, and brown bars, did not exhibit any differences in their jumping performance regardless of their previous concussion history. In contrast, the group that did sustain a concussion year-to-year, represented by the green, red, pink, and grey bars, showed extremely similar year-to-year IJV levels for this metric if they had no previous concussion history. However, those with a history of concussions had significantly higher year-to-year IJV levels for max ankle distance. All other metrics returned no significantly discriminatory results for IJV. The results of the prospective study suggest that despite recent mTBI injury or presence of concussion history or lack thereof, athletes IJV remains relatively the same before and after injury apart from a few notable distinctions.

4.5 Feature Selection by Machine Learning Classifiers

When dealing with large datasets with high dimensionality in machine learning, feature selection is a technique used by researchers and engineers to remove irrelevant data [64]. In other words, after the feature selection process is complete, we are left with the most important features in the dataset that lead to the highest performance for the specific machine learning task (regression, classification, etc.). The goal of this section of the research is to test different machine learning classifiers to see which one performs best at identifying those who have had a concussion in the last two years and those who have not. The classification task is purely binary. To do this, we apply an iterative, exhaustive approach where each feature is tested one by one in the binary classification task. Whichever feature yields the highest balanced accuracy score, which is defined as the average

of recall obtained on each class, is selected as a ‘best feature’. The next iteration performs the same binary classification task but this time with the previously found best feature and tests every other feature one-by-one in tandem with the previous best feature(s) and whichever feature yields the best-balanced accuracy is selected as the next best feature. This process repeats iteratively 14 times until we have a list of 14 best features for our dataset given the binary classification task. This strategy is employed to provide us with insights on which are the most important metrics KITS outputs for each exercise given the binary classification task of identifying recently concussed athletes. The four classifiers being tested are SVM, KNN, MLP and random forest (RF) decision tree classifiers and will be compared based on precision, recall, F1-score, and total accuracy. Synthetic Minority Oversampling Technique (SMOTE) resampling has been used for all tests since the dataset is severely imbalanced towards the control group. SMOTE resampling is a common approach used to address imbalanced datasets by duplicating examples in the minority class without adding any new information to the model [65]. A 70/30 train/test split was used for all tests and no standardization was applied to the dataset. Table 17 shows the comparative results for the DVJ exercise on the binary classification task for all four classifiers.

Table 17 Machine Learning Classifier Results for DVJ (binary classification task)

Classifier Type	Group	Precision	Recall	F1-score	Support
SVM	Control	0.94	0.42	0.58	109
	Concussed	0.28	0.89	0.43	28
	Accuracy			0.52	
KNN	Control	0.86	0.52	0.65	109
	Concussed	0.27	0.68	0.38	28
	Accuracy			0.55	
MLP	Control	0.85	0.79	0.82	109
	Concussed	0.36	0.46	0.41	28
	Accuracy			0.72	
Random Forest Decision Tree	Control	0.82	0.89	0.85	109
	Concussed	0.37	0.25	0.3	28
	Accuracy			0.76	

The results demonstrate that the random forest decision tree has the highest absolute accuracy after selecting the 14 best features compared to all other classifiers. However, the random forest decision tree classifier has the worst macro recall score out of the four, meaning that it produces the most number of false negatives. The KNN classifier performs well on the concussed group in terms of recall but less well in terms of accuracy. The SVM classifier has the worst overall accuracy score and has very poor recall for the control group but performs surprisingly well in terms of recall for the concussed group but very poorly in terms of precision. The MLP classifier seems to perform the best with an overall accuracy of 0.72, acceptable recall and precision scores for the control and low, albeit comparatively adequate precision and recall scores for the concussed group. Figure 32 shows the balanced accuracy of all four classifiers at each iteration of the feature selection process.

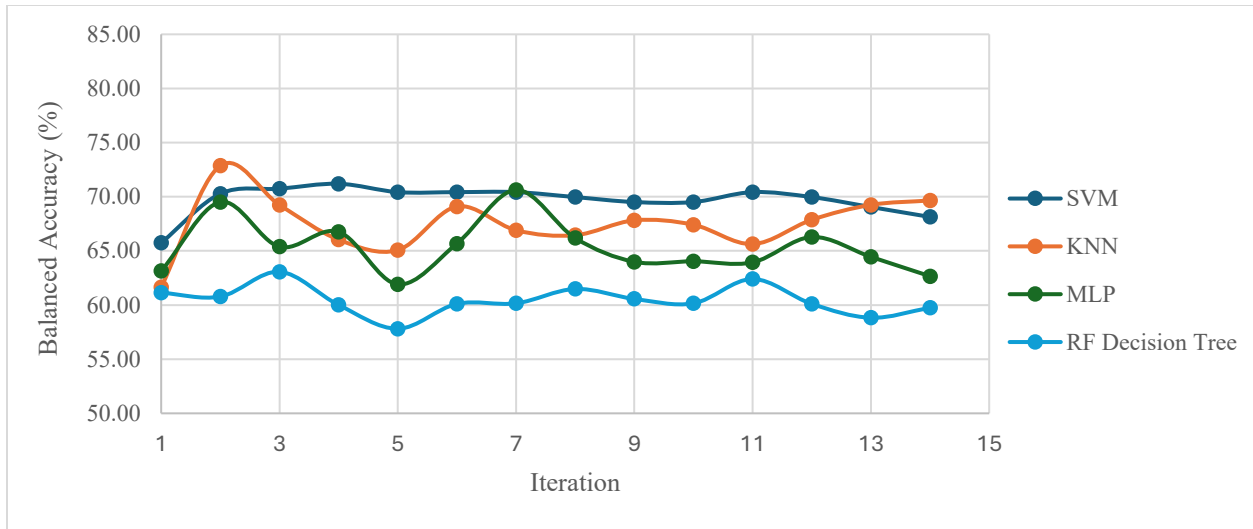


Figure 32 Balanced Accuracy (%) for each classifier for feature selection process (DVJ)

The RF decision tree performs consistently poorly in terms of balanced accuracy score throughout the entire feature selection process. The MLP classifier performs well up until it selects the 7th feature, afterwards its accuracy score continues to drop. The SVM classifier performs consistently well, but slowly drops after the 11th best feature is selected. The KNN classifier finishes with the top balanced accuracy score after 14 features have been selected. Table 18 reports on the selected best features for the best performing MLP classifier.

Table 18 Best Features for MLP Classifier (DVJ)

Iteration	Feature Name	Balanced Accuracy (%)
1	Max Pelvis Tilt Z	63.14
2	Mid Axis Sway Ratio	69.51
3	Max Wrist Distance	65.38
4	Max Ankle Distance	66.76
5	Peak Valgus Left	61.91
6	Peak Coronal Right	65.68
7	Time to Stabilization	70.63
8	Spine Sway Variability Landing Ratio Z	66.19
9	Spine Sway X Variability	63.99
10	Spine Sway Variability Landing Ratio X	64.04
11	Peak Valgus Right	63.94
12	Max Pelvis Tilt Y	66.28
13	Max Spine Sway X	64.45
14	Initial Coronal Left	62.66

The results demonstrate that the MLP classifier’s balanced accuracy score falls off after selecting time to stabilization as the 7th best feature, indicating that the selected features after it are detrimental to the binary classification task of classifying a history of recent concussion.

The same study was conducted for SLS, this time only considering exercise recordings performed on the dominant leg for the sake of simpler and more concise analysis. Table 19 shows the comparative results for the SLS exercise on the binary classification task for all four classifiers.

Table 19 Machine Learning Classifier Results for SLS Dominant Leg (binary classification task)

Classifier	Group	Precision	Recall	F1-score	Support
SVM	Control	0.85	0.33	0.48	106
	Concussed	0.19	0.74	0.31	23
	Accuracy			0.4	
KNN	Control	0.87	0.55	0.67	106
	Concussed	0.23	0.61	0.33	23
	Accuracy			0.56	
MLP	Control	0.82	0.61	0.7	106
	Concussed	0.18	0.39	0.25	23
	Accuracy			0.57	
Random Forest Decision Tree	Control	0.84	0.92	0.88	106
	Concussed	0.38	0.22	0.28	23
	Accuracy			0.8	

The results once again demonstrate that the random forest decision tree model has the highest absolute accuracy rating out of all classifiers. The SVM classifier stands out by performing particularly poorly with an accuracy rating half that of the random forest decision tree model and very poor recall scores for the control group and terrible precision score for the concussed group. MLP and KNN both present adequate recall scores for both the concussed and control groups but each perform poorly in terms of precision for both groups. Figure 33 shows the balanced accuracy scores of each model during the feature selection process.

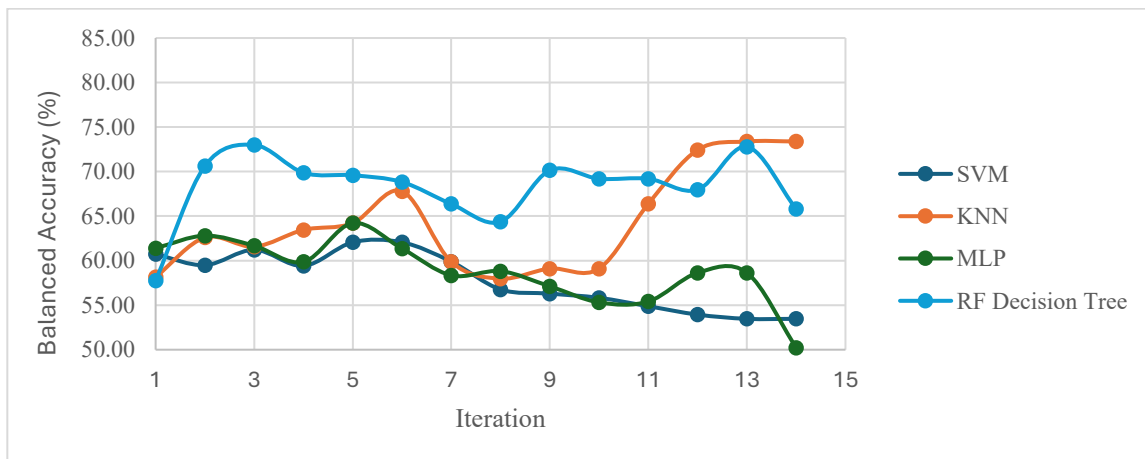


Figure 33 Balanced Accuracy (%) for each classifier for feature selection process (SLS)

The results demonstrate that the MLP and SVM classifiers both perform poorly as more features are added to the stack throughout the feature selection process, both dropping below a

55% balanced score accuracy. On the other hand, the KNN and RF decision tree classifier are the best performers with KNN edging out the RF decision tree at the 14th best selected feature. However, both KNN and RF decision tree performed similarly after 13 feature selections. The RF decision tree's similar performance based on balance accuracy to the KNN classifier and superior overall accuracy of 0.8 compared to KNN's 0.56 make it the best performing machine learning classifier candidate for the SLS. The chosen features by the random forest classifier for the SLS are shown in Table 20.

Table 20 Best Features for RF Decision Tree Classifier (SLS)

Iteration	Feature Name	Balanced Accuracy (%)
1	Mid Axis Sway Ratio	57.77
2	Max Pelvis Tilt Y	70.63
3	Peak Sagittal Second	72.99
4	NSL Max Sagittal	69.87
5	Max Neck Sway X	69.59
6	Max Pelvis Tilt Z	68.83
7	TBCM Sway	66.37
8	Max Spine Sway X	64.38
9	NSL Coronal Variability	70.14
10	Max Wrist Distance	69.20
11	Initial Coronal First	69.20
12	NSL Sagittal Variability	67.97
13	Time To Stabilization	72.79
14	Peak Sagittal First	65.79

The RF decision tree classifier's balance accuracy performance improves and maximizes until the 13th selected feature: time to stabilization. Peak sagittal of the first squat reduces the balanced accuracy by 7%, suggesting that the metric is less valuable in the task of classifying recently concussed athletes. The NSL shows up three times in the top 14 features suggesting that the metrics of the NSL are important in assessing recently concussed athletes. Many sway metrics also make an appearance such as TBCM sway, maximum neck and spine sway further suggesting the sway metrics play an important role in assessing concussion history. Pelvis tilt in both the X and Z directions also make an appearance which indicates the athlete's pelvis tilt influences whether they get classified as a recently concussed individual from the machine leaning model.

The same study was conducted for the SLH, also only considering exercise recordings performed on the dominant leg for the sake of simpler and more concise analysis. Table 21 shows the comparative results for the SLH exercise on the binary classification task for all four classifiers.

Table 21 Machine Learning Classifier Results for SLH Dominant Leg (binary classification task)

Classifier	Group	Precision	Recall	F1-score	Support
SVM	Control	0.95	0.47	0.63	120
	Concussed	0.1	0.7	0.17	10
				Accuracy	0.48
KNN	Control	0.93	0.58	0.72	120
	Concussed	0.09	0.5	0.15	10
				Accuracy	0.64
MLP	Control	0.93	0.79	0.86	120
	Concussed	0.11	0.3	0.16	10
				Accuracy	0.75
Random Forest Decision Tree	Control	0.93	0.93	0.93	120
	Concussed	0.18	0.2	0.19	10
				Accuracy	0.87

The results demonstrate that the RF decision tree performs the best in terms of absolute accuracy compared to all other models. The SLH has less support for the concussed group compared to the DVJ and SLS since we had less reported concussions in 2022 compared to 2023. The increased imbalance of the dataset leads to very poor recall and precision values for the concussed group for all machine learning classifiers. Where the recall was much improved, in cases demonstrated by the SVM and KNN classifiers, the accuracy of the control group decreased significantly compared to other models. F1-scores for the concussed group were poor across the board for all classifiers. Figure 34 shows the balanced accuracy scores for each model during the feature selection process.

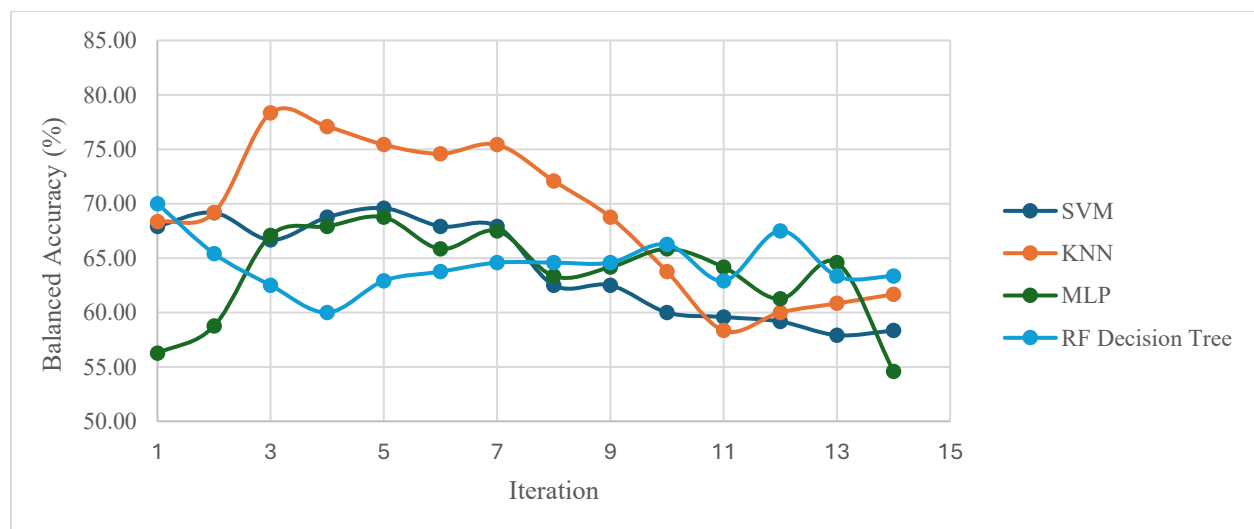


Figure 34 Balanced Accuracy (%) for each classifier for feature selection process (SLH)

The balanced accuracy results demonstrate that the KNN classifier initially performs very strongly compared to the other classifiers. However, this is mainly due to KNN not producing

many false negatives for each class early on but performing poorly based on precision and F1-score for the concussed cohort. As more features get added to the stack, the KNN classifier's balanced accuracy falls due to it producing more false negatives. All other classifiers remain comparably flat in their performance throughout the feature selection process never achieving a balanced accuracy above 70%. Because of the KNNs initial strong performance with small number of features at classifying recently concussed athletes, it is selected as the best performing classifier for the SLH. The chosen features by the random forest classifier for the SLH are shown in Table 22.

Table 22 Best Features for RF Decision Tree Classifier (SLS)

Iteration	Feature Name	Balanced Accuracy (%)
1	NSL Sagittal Variability	68.33
2	Max Pelvis Tilt Y	69.17
3	NSL Coronal Variability	78.33
4	Mid Axis Sway Ratio	77.08
5	Max Ankle Distance	75.42
6	Time to Stabilization	74.58
7	Spine Sway X Variability	75.42
8	SL Coronal Variability	72.08
9	Spine Sway Z Variability	68.75
10	Max Wrist Distance	63.75
11	Max Spine Sway X	58.33
12	NSL Maximum Coronal	60.00
13	Max Spine Sway Z	60.83
14	Peak Coronal	61.67

The results once again demonstrate that the NSL metrics are important in distinguishing between those with a history of recent concussion and those without. NSL sagittal and coronal variability both show up in the top three selected features along with maximum pelvis tilt in the Y direction. After selecting the aforementioned three features, the balanced accuracy of the model falls dramatically to 58.33% at the 11th best feature until rising slightly after adding another NSL metric in maximum coronal angle. The classification report using only the top three features found by the feature selection show that the KNN classifier performs the best compared to all other classifiers for the SLH with very small dimensionality, albeit still with poor precision and F1-score for the concussed group due to high dataset imbalance. These results are shown in Table 23.

Table 23 Classification Report for KNN using top three features (SLH)

Group	Precision	Recall	F1-score	Support
Control	0.98	0.54	0.7	120
Concussed	0.14	0.9	0.24	10
Accuracy			0.57	

Chapter 5 Conclusions and Future Work

The goal of our research was to ascertain any notable distinctions in the movement mechanics and balance capabilities of varsity athletes using pose estimation software and assess which of the three examined exercises most exemplify these distinctions. The results of the experiment demonstrate that the DVJ is most suitable in distinguishing movement mechanics between concussed and healthy individuals returning eleven body angles which significantly decreased between groups suggesting stiffer overall movement for the concussed group compared to the control. The most significant finding was the concussed group having a higher overall TTS than the control group for the DVJ [mean difference = 0.089 seconds, $p = 0.046$]. The findings indicate that the SLS and SLH may not be as effective in identifying concussion history, as they only yielded two and three metrics, respectively, that showed significant differences between the groups. Most notably, the concussed athletes had a lower average TTS on the dominant leg compared to the control group [mean difference = 0.048 seconds, $p = 0.026$] for the SLH which is opposite to the expected trend. This outcome could be a result of concussed varsity athletes at McGill University having better overall balance on one leg after undergoing a specific and coordinated concussion rehabilitation program than those who did not.

The research also prospectively examined a group of 20 varsity athletes which performed at least three drop vertical jumps in both 2022 and 2023 and sustained one or many concussions from year to year to ascertain any mechanical or dynamic balance differences between their pre- and post-injury jumps. The results of the experiment demonstrate no statistically significant differences between their 2022 and 2023 jumps for all computed metrics except for notably lower mean peak sagittal left, right and maximum spine sway X angles. This may be due to dynamic balance deficits observed in the injured athletes, leading to their reluctance to squat to their fullest potential when performing a DVJ after recovering from a mTBI. Intra-jump variability was also examined, and the results showed significant increases in jump-to-jump variability for peak sagittal left & right angles, spine sway variability in the Z direction and maximum ankle distance. This further suggests potential disruptions in neuromuscular control or balance, indicating that the mTBI has had a lasting impact on their motor coordination and stability.

Four machine learning classifiers were used to perform exhaustive feature selection for the DVJ, SLS and SLH to determine which metrics are most important at distinguishing between concussed and control groups. The results of the experiments demonstrate that the MLP classifier was most adept at distinguishing between groups for the DVJ and its balance accuracy score increased steadily when adding features to the stack until the introduction of time to stabilization, whereafter it decreased. Furthermore, the RF decision tree model performed best for the SLS which presented many NSL and sway metrics as top features when classifying concussed athletes, suggesting those to be important in distinguishing between injured and non-injured participants. Moreover, the KNN classifier performed well for the SLH with low dimensionality and also presented many NSL metrics as top features, further suggesting that monitoring the behavior of the NSL is an important aspect in distinguishing between injured and non-injured athletes.

A gender-based analysis was performed to ascertain which aerobic exercise best discriminates between concussed and healthy controls for males and females. The results of the experiment

demonstrated that the DVJ was more adept at distinguishing mechanical differences between injured and healthy athletes for males returning eleven discriminatory metrics but much less effective for females returning only one significant metric. Overall, the SLS was the least effective exercise in discriminating between concussed and healthy controls for both males and females returning only one statistically significant metric for both sexes. Finally, for females, the SLH proved to be most adept at identifying mechanical differences between concussed and healthy controls returning five significant discrepancies on the dominant leg and six on the non-dominant leg whereas only returned one significantly different metric for both the dominant and non-dominant legs for males.

This research was limited by the atomic ‘one-shot’ nature of the dataset which only examines athlete exercises during pre-season physicals. None of the athletes performing exercises were concussed or very recently recovered from injury at the time of data collection. A prospective study which collects exercise data of athletes several times throughout the course of the season is suggested for more concrete results at detecting concussion history. Furthermore, our study was limited by the available power in our regression models for GRF prediction, especially for the SLH which we were unable to collect force plate data of the subjects jumping onto the force plate. A study which bolsters the number of subjects jumping onto the force plate should produce more accurate GRF regression models and thus increase the accuracy of estimated time to stabilization for the three exercises. Lastly, our dataset was limited by its imbalanced nature. This issue was especially evident when training machine learning classifiers to detect athletes with a history of concussion in the binary classification task. A study which thoroughly addresses class imbalance could potentially yield more accurate and reliable models, enhancing the robustness of concussion detection in athletic populations.

Future work will have to explore methods for how to implement the results of this research in practical settings. A practical implementation of our research can be scoring how well an athlete has recovered from their mild traumatic brain injury. Since we know time to stabilization increases for injured athletes who perform a DVJ, scoring a recovered athletes’ time to stabilization relative to the known injured threshold can give medical professionals decision support on how well an athlete has recovered from their mTBI based on their dynamic balance capabilities. Furthermore, we can score concussion injury probability of a suspected injured athlete. Since we know which metrics for which exercises are significantly different between injured and non-injured athletes, athletes that return similar significantly different metrics to the known concussion identifiers would be scored more severely for injury probability.

Bibliography

- [1] C. A. Abeare, et al., "Prevalence of invalid performance on baseline testing for sport-related concussion by age and validity indicator," *Jama Neurology*, vol. 75, no. 6, pp. 697, 2018. [Online]. Available: <https://doi.org/10.1001/jamaneurol.2018.0031>.
- [2] Chhabra, "Baseline Concussion Testing Keeps Athletes Game Ready," *Global Sport Matters*, 30 July 2018. [Online]. Available: <https://globalsportmatters.com/health/2018/07/30/baselineconcussion-testingkeepsathletesgameready/#:~:text=The%20K%2DD%20test%20is%20a,which%20take%20about%20two%20minutes>.
- [3] H.-H. Hsu, W.-H. Lai, H.-T. Yu, S.-H. Xiao, Y.-H. Tsai, K.-C. Wang, S.-J. Huang, C.-C. Yang, "Long-Term Presentation of Postconcussion Symptoms and Associated Factors: Analysis of Latent Class Modeling," *Archives of Clinical Neuropsychology*, vol. 36, no. 1, pp. 62–73, Feb. 2021. [Online]. Available: <https://doi.org/10.1093/arclin/acia063>.
- [4] A. A. Oyekan, S. Eagle, A. M. Trbovich, J. D. Shaw, M. Schneider, M. Collins, J. Y. Lee, and A. P. Kontos, "Neck Symptoms and Associated Clinical Outcomes in Patients Following Concussion," *Journal of Head Trauma Rehabilitation*, vol. 38, no. 6, pp. 417-424, Nov./Dec. 2023. DOI: 10.1097/HTR.0000000000000866.
- [5] L. Lowe, F. Castillo, Y. Gokun, D. K. Williams, M. Israel, and C. Yates, "Static and Dynamic Balance Assessment in Healthy and Concussed Adolescent Athletes," *Clin J Sport Med*, vol. 32, no. 4, pp. 385-390, Jul. 2022. DOI: 10.1097/JSM.0000000000000979. Epub Sep. 28, 2021. PMID: 34596064; PMCID: PMC8958180.
- [6] APTA, "Balance Error Scoring System (BESS)," [Online]. Available: www.apta.org/patient-care/evidence-based-practice-resources/test-measures/balance-error-scoring-system-bess#:~:text=The%20Balance%20Error%20Scoring%20System,or%20mild%20traumatic%20brain%20injury. Accessed: Feb. 26, 2024.
- [7] R. D. Patel and C. R. LaBella, "Contributions of PCSS, BESS, Tandem Gait, and Romberg Test for Identifying Balance Deficits in Pediatric Concussions," *Journal of Head Trauma Rehabilitation*, vol. 37, no. 2, pp. E129-E134, Mar./Apr. 2022. DOI: 10.1097/HTR.0000000000000702.
- [8] M. Zhu, Z. Huang, C. Ma, and Y. Li, "An Objective Balance Error Scoring System for Sideline Concussion Evaluation Using Duplex Kinect Sensors," *Sensors (Basel)*, vol. 17, no. 10, pp. 2398, Oct. 20, 2017. DOI: 10.3390/s17102398. PMID: 29053602; PMCID: PMC5677441.
- [9] IBM, "What Is Computer Vision?" [Online]. Available: www.ibm.com/topics/computer-vision.
- [10] S. C. Babu, "A 2019 Guide to Human Pose Estimation with Deep Learning," in *Proceedings of the IEEE Conference on Computer Vision and Pattern Recognition*, pp. 11977–11986, 2019.
- [11] J. Stenum, K. M. Cherry-Allen, C. O. Pyles, R. D. Reetzke, M. F. Vignos, and R. T. Roemmich, "Applications of Pose Estimation in Human Health and Performance across the Lifespan," *Sensors (Basel)*, vol. 21, no. 21, pp. 7315, Nov. 2021. doi: 10.3390/s21217315.
- [12] L. Zatolokina, "Computer Vision and Pose Estimation for Fitness / Rehab Therapy Apps," *MobiDev*, Jan. 19, 2024. [Online]. Available: mobidev.biz/blog/human-pose-estimation-technology-guide.

- [13] M. Andriluka, L. Pishchulin, P. Gehler, and B. Schiele, "2D Human Pose Estimation: New Benchmark and State of the Art Analysis," in *Proceedings of the IEEE Computer Society Conference on Computer Vision and Pattern Recognition*, Columbus, OH, USA, 23–28 June 2014, pp. 3683–3693.
- [14] Microsoft. "Azure Kinect and Kinect Windows v2 Comparison." Microsoft.Com, 7 July 2023. [Online]. Available: learn.microsoft.com/en-us/azure/kinect-dk/windows-comparison. Accessed: 27 February 2024.
- [15] J. McCormick, "How does the Kinect Work," University of Wisconsin, Madison, WI, [Online]. Available: <https://pages.cs.wisc.edu/~ahmad/kinect.pdf>. Accessed: 27 February 2024
- [16] L. Yang, et al., "Evaluating and improving the depth accuracy of Kinect for Windows V2," *IEEE Sensors Journal*, vol. 15, no. 8, pp. 4275–4285, Aug. 2015. DOI: 10.1109/JSEN.2015.2416651.
- [17] Shotton, Jamie, et al. "Real-Time Human Pose Recognition in Parts from Single Depth Images," *Communications of the ACM*, vol. 56, no. 1, pp. 116–124, 2013. [DOI: 10.1145/2398356.2398381]
- [18] Raj, Ashwin. "An Exhaustive Guide to Decision Tree Classification in Python 3.X," *Medium, Towards Data Science*, 11 Dec. 2021, [URL: towardsdatascience.com/an-exhaustive-guide-to-classification-using-decision-trees-8d472e77223f].
- [19] Darby, John, et al. "An Evaluation of 3D Head Pose Estimation Using the Microsoft Kinect V2," *Gait & Posture*, vol. 48, pp. 83–88, 2016. DOI: 10.1016/j.gaitpost.2016.04.030.
- [20] Kurillo G, Hemingway E, Cheng ML, Cheng L. "Evaluating the Accuracy of the Azure Kinect and Kinect v2," *Sensors (Basel)*, vol. 22, no. 7, pp. 2469, Mar 23, 2022. DOI: 10.3390/s22072469. PMID: 35408082; PMCID: PMC9002889.
- [21] Silverberg ND, Iaccarino MA, Panenka WJ, Iverson GL, McCulloch KL, Dams-O'Connor K, Reed N, McCrea M; American Congress of Rehabilitation Medicine Brain Injury Interdisciplinary Special Interest Group Mild TBI Task Force. "Management of Concussion and Mild Traumatic Brain Injury: A Synthesis of Practice Guidelines," *Arch Phys Med Rehabil*, vol. 101, no. 2, pp. 382-393, Feb 2020. DOI: 10.1016/j.apmr.2019.10.179. PMID: 31654620.
- [22] Mild Traumatic Brain Injury Committee, A. C. R. M. "Definition of mild traumatic brain injury," *J Head Trauma Rehabil*, vol. 8, no. 3, pp. 86-87, 1993.
- [23] Tjong VK, Baker HP, Cogan CJ, Montoya M, Lindley TR, Terry MA. "Concussions in NCAA Varsity Football Athletes: A Qualitative Investigation of Player Perception and Return to Sport," *J Am Acad Orthop Surg Glob Res Rev*, vol. 1, no. 8, pp. e070, Nov 20, 2017. DOI: 10.5435/JAAOSGlobal-D-17-00070. PMID: 30211371; PMCID: PMC6132341.
- [24] Higgins KL, Denney RL, Maerlender A. "Sandbagging on the Immediate Post-Concussion Assessment and Cognitive Testing (ImpACT) in a high school athlete population," *Arch Clin Neuropsychol*, vol. 32, no. 3, pp. 259-266, May 1, 2017. DOI: 10.1093/arclin/acw108. PMID: 28431031.
- [25] Stern, Rachel. "Outsmarting the Test: Concussions & ImpACT," *ButlerStories, Butler University*, Jul 31, 2018, [URL: stories.butler.edu/outsmarting-the-test-concussions-impact/].
- [26] Kerr ZY, Roos KG, Djoko A, Dalton SL, Broglio SP, Marshall SW, Dompier TP. "Epidemiologic Measures for Quantifying the Incidence of Concussion in National Collegiate Athletic Association Sports," *J Athl Train*, vol. 52, no. 3, pp. 167-174, Mar 2017.

DOI: 10.4085/1062-6050-51.6.05. Epub 2016 Jun 22. PMID: 27331336; PMCID: PMC5384815.

- [27] Concussion Legacy Foundation, "What Is PCS?" Concussion Legacy Foundation. [Online]. Available: concussionfoundation.org/PCS-resources/what-is-PCS?gad_source=1&gclid=Cj0KCQiA84CvBhCaARIsAMkAvkJhuDL3yDGdVSQDCBbPe nAjvaGHjSZ4ciIquCCvKQZSYeE9Pc4oP4QaAk9SEALw_wcB. Accessed: Feb. 29, 2024.
- [28] J. Leddy et al., "Management of Concussion and Persistent Post-Concussive Symptoms for Neurologists," *Curr Neurol Neurosci Rep.*, vol. 21, no. 12, p. 72, Nov. 24, 2021, doi: 10.1007/s11910-021-01160-9, PMID: 34817719.
- [29] O. H. Skjeldal et al., "Long-term post-concussion symptoms," *Tidsskr Nor Laegeforen*, vol. 142, no. 12, Aug. 17, 2022, doi: 10.4045/tidsskr.21.0713, PMID: 36066235.
- [30] J. Leddy et al., "Clinical Assessment of Concussion and Persistent Post-Concussive Symptoms for Neurologists," *Current Neurology and Neuroscience Reports*, vol. 21, no. 12, 2021, doi: 10.1007/s11910-021-01159-2.
- [31] T. A. Buckley et al., "Sensitivity and Specificity of the Modified Balance Error Scoring System in Concussed Collegiate Student Athletes," *Clinical Journal of Sport Medicine*, vol. 28, no. 2, pp. 174–176, 2018, doi: 10.1097/JSM.0000000000000426.
- [32] B. J. Lee et al., "Movement patterns during a jump-landing task in athletes after sport-related concussion and healthy control individuals," *Journal of Athletic Training*, vol. 56, no. 12, pp. 1306–1312, Feb. 24, 2021, doi: 10.4085/533-20.
- [33] A. P. Lapointe et al., "Kinematic differences during a jump cut maneuver between individuals with and without a concussion history," *Int J Psychophysiol*, vol. 132, pt A, pp. 93–98, 2018.
- [34] D. F. Dubose et al., "Lower extremity stiffness changes after concussion in collegiate football players," *Med Sci Sport Exerc*, vol. 49, no. 1, pp. 167–172, 2017, doi: 10.1249/MSS.0000000000001067.
- [35] J. Leddy et al. "Early subthreshold aerobic exercise for sport-related concussion." *JAMA Pediatrics*, vol. 173, no. 4, 1 Apr. 2019, p. 319, <https://doi.org/10.1001/jamapediatrics.2018.4397>.
- [36] L. Brown and J. Camarinos, "The Role of Physical Therapy in Concussion Rehabilitation," *Semin Pediatr Neurol*, vol. 30, pp. 68-78, Jul. 2019, doi: 10.1016/j.spen.2019.03.011.
- [37] R. C. Lynall, K. R. Campbell, T. C. Mauntel, J. T. Blackburn, and J. P. Mihalik, "Single-Legged Hop and Single-Legged Squat Balance Performance in Recreational Athletes With a History of Concussion," *J. Athl. Train.*, vol. 55, no. 5, pp. 488-493, May 2020. doi: 10.4085/1062-6050-185-19. [Online]. Available: <https://pubmed.ncbi.nlm.nih.gov/32216655/>
- [38] Z. Ripic et al., "Ground reaction force and joint moment estimation during gait using an Azure Kinect-driven musculoskeletal modeling approach," *Gait & Posture*, vol. 95, pp. 49-55, Jun. 2022. doi: 10.1016/j.gaitpost.2022.04.005.
- [39] Eltoukhy, Moataz, et al. "Prediction of Ground Reaction Forces for Parkinson's Disease Patients Using a Kinect-Driven Musculoskeletal Gait Analysis Model." *Medical Engineering & Physics*, vol. 50, 2017, pp. 75–82, <https://doi.org/10.1016/j.medengphy.2017.10.004>.
- [40] AnyBody Technology, "The Anybody Modeling System," [Online]. Available: <http://www.anybodytech.com/software/anybodymodelingsystem/>. Accessed: Apr. 11, 2023.
- [41] A. Kleiner et al., "The Coefficient of Friction in Parkinson's Disease Gait," *Functional Neurology*, vol. 32, no. 1, pp. 17-22, 2017.

- [42] A. Ardalan, N. Yamane, A. K. Rao, J. Montes, and S. Goldman, "Analysis of Gait Synchrony and Balance in Neurodevelopmental Disorders Using Computer Vision Techniques," *Health Informatics J.*, vol. 27, no. 4, pp. 14604582211055650, Oct.-Dec. 2021. doi: 10.1177/14604582211055650.
- [43] L. F. Yeung, K. C. Cheng, C. H. Fong, W. C. C. Lee, and K.-Y. Tong, "Evaluation of the Microsoft Kinect as a Clinical Assessment Tool of Body Sway," *Gait & Posture*, vol. 40, no. 4, pp. 532-538, 2014. ISSN 0966-6362. doi: 10.1016/j.gaitpost.2014.06.012. [Online]. Available: <https://www.sciencedirect.com/science/article/pii/S0966636214006122>.
- [44] D. A. Winter, "Biomechanics and Motor Control of Human Movement" 4th ed. Canada: John Wiley & Sons, Inc., 2009.
- [45] Y. Yang, F. Pu, Y. Li, S. Li, Y. Fan and D. Li, "Reliability and Validity of Kinect RGB-D Sensor for Assessing Standing Balance," in *IEEE Sensors Journal*, vol. 14, no. 5, pp. 1633-1638, May 2014, doi: 10.1109/JSEN.2013.2296509.
- [46] M. Z. Rodriguez, et al., "Clustering Algorithms: A Comparative Approach," **PLOS ONE**, [Online]. Available: <https://journals.plos.org/plosone/article?id=10.1371/journal.pone.0210236>. Accessed: Mar. 4, 2024.
- [47] S. Jaiswal, "Multilayer Perceptrons in Machine Learning: A Comprehensive Guide," DataCamp, Feb. 7, 2024. [Online]. Available: www.datacamp.com/tutorial/multilayer-perceptrons-in-machine-learning.
- [48] M. A. Awadallah, I. Abu-Doush, M. A. Al-Betar, and M. S. Braik, "Metaheuristics for optimizing weights in neural networks," in *Comprehensive Metaheuristics*, S. Mirjalili and A. H. Gandomi, Eds. Academic Press, 2023, pp. 359-377, doi: 10.1016/B978-0-323-91781-0.00005-3.
- [49] J. Naskath, G. Sivakamasundari, and A. S. Begum, "A Study on Different Deep Learning Algorithms Used in Deep Neural Nets: MLP SOM and DBN," *Wireless Pers. Commun.*, vol. 128, pp. 2913-2936, 2023, doi: 10.1007/s11277-022-10079-4.
- [50] J. Cervantes, F. Garcia-Lamont, L. Rodríguez-Mazahua, and A. Lopez, "A Comprehensive Survey on Support Vector Machine Classification: Applications, Challenges and Trends," **Neurocomputing**, vol. 408, pp. 189-215, 2020, ISSN 0925-2312, doi: 10.1016/j.neucom.2019.10.118. [Online]. Available: <https://www.sciencedirect.com/science/article/pii/S0925231220307153>.
- [51] IBM, "What Is the K-Nearest Neighbors Algorithm?" [Online]. Available: [www.ibm.com/topics/knn#:~:text=The%20k%2Dnearest%20neighbors%20\(KNN\)%20algorithm%20is%20a%20non,of%20an%20individual%20data%20point](http://www.ibm.com/topics/knn#:~:text=The%20k%2Dnearest%20neighbors%20(KNN)%20algorithm%20is%20a%20non,of%20an%20individual%20data%20point). Accessed: Mar. 5, 2024.
- [52] K. Taunk, S. De, S. Verma, and A. Swetapadma, "A Brief Review of Nearest Neighbor Algorithm for Learning and Classification," in **Proceedings of the 2019 International Conference on Cyber Security and Protection of Digital Services (ICCS)**, pp. 1255-1260, 2019, doi: 10.1109/ICCS45141.2019.9065747.
- [53] N. Liberman, "Decision Trees and Random Forests," **Medium**, Towards Data Science, May 21, 2020. [Online]. Available: towardsdatascience.com/decision-trees-and-random-forests-df0c3123f991.
- [54] Y. Song and Y. Lu, "Decision Tree Methods: Applications for Classification and Prediction," **Shanghai Arch Psychiatry**, vol. 27, no. 2, pp. 130-135, Apr. 25, 2015. doi: 10.11919/j.issn.1002-0829.215044. PMID: 26120265; PMCID: PMC4466856.

- [55] A. G. Ganie and S. Dadvandipour, "From Big Data to Smart Data: A Sample Gradient Descent Approach for Machine Learning," **Journal of Big Data**, vol. 10, p. 162, 2023. [Online]. Available: <https://doi.org/10.1186/s40537-023-00839-9>.
- [56] R. Malhotra Kumar, "Linear Regression: Modeling and Assumptions," **Medium**, Towards Data Science, Sept. 30, 2018. [Online]. Available: towardsdatascience.com/linear-regression-modeling-and-assumptions-dcd7a201502a.
- [57] J. N. Wilder, E. R. Riggins, R. A. Noble, C. M. Lelito, T. L. Widenhoefer, T. G. Almonroeder, "The effects of drop vertical jump technique on landing and jumping kinetics and jump performance," *Journal of Electromyography and Kinesiology*, vol. 56, pp. 102504, 2021. ISSN 1050-6411. DOI: 10.1016/j.jelekin.2020.102504.
- [58] L. Jamhoury, "Understanding Kinect v2 Joints and Coordinate System," Medium, Apr. 21, 2022. [Online]. Available: lisajamhoury.medium.com/understanding-kinect-v2-joints-and-coordinate-system-4f4b90b9df16. [Accessed: Apr. 30, 2024].
- [59] D. P. Fransz, A. Huurnink, V. A. de Boode, I. Kingma, and J. H. van Dieën, "Time to stabilization in single leg drop jump landings: an examination of calculation methods and assessment of differences in sample rate, filter settings and trial length on outcome values," *Gait Posture*, vol. 41, no. 1, pp. 63-69, Jan. 2015. [Online]. Available: 10.1016/j.gaitpost.2014.08.018. [Accessed: Mar. 6, 2024].
- [60] S. Ocklenburg, "5 Scientific Facts about Left-Footedness," *Psychology Today*, Feb. 15, 2020. [Online]. Available: www.psychologytoday.com/ca/blog/the-asymmetric-brain/202002/5-scientific-facts-about-left-footedness#:~:text=Overall%2C%20there%20were%2061.6%20percent,than%20mixed%2Dhanded%20or%20ambidextrous.
- [61] L. Li, "Time of Flight Camera - An Introduction," Texas Instruments, Jan. 2014.
- [62] Starling AJ, Leong DF, Bogle JM, Vargas BB, "Variability of the modified Balance Error Scoring System at baseline using objective and subjective balance measures". *Concussion*. 2015 Aug 6;1(1):CNC5. doi: 10.2217/cnc.15.5. PMID: 30202550; PMCID: PMC6114022.
- [63] Damjanovic, Jelena. "Starting Aerobic Exercise Soon after Concussion Improves Recovery Time, U of T Study Finds." University of Toronto, 19 Apr. 2018. [Online]. Available: www.utoronto.ca/news/starting-aerobic-exercise-soon-after-concussion-improves-recovery-time-u-t-study-finds#:~:text=Lawrence%20suggests%20initially%20doing%20low,they%20involve%20greater%20head%20movement. [Accessed: May 21, 2024]
- [64] J. Cai, S. Chen, L. Hu, Y. Chen, and Z. Chen, "Feature selection in Machine Learning: A new perspective," *Neurocomputing*, vol. 300, pp. 70-79, Jul. 2018, doi: 10.1016/j.neucom.2017.11.077.
- [65] J. Brownlee, "Smote for Imbalanced Classification with Python," *MachineLearningMastery.Com*, Mar. 17, 2021. [Online]. Available: <https://machinelearningmastery.com/smote-oversampling-for-imbalanced-classification/>.
- [66] "What Is Random Forest?" IBM, Oct. 20, 2021. [Online]. Available: www.ibm.com/topics/random-forest#:~:text=Random%20forest%20is%20a%20commonly,both%20classification%20and%20regression%20problems.